Journal of Mathematical Biology (2024) 88:34
https://doi.org/10.1007/s00285-024-02056-1

Mathematical Biology

Three-stage modeling of HIV infection and implications for antiretroviral therapy

Cameron Clarke[1] · Stephen Pankavich[1]

Received: 25 July 2023 / Revised: 1 December 2023 / Accepted: 28 January 2024

Abstract
We consider a deterministic model of HIV infection that involves macrophages as a long-term active reservoir to describe all three stages of the disease process: the acute stage, chronic infection, and the transition to AIDS. The proposed model is shown to retain crucial properties, such as the positivity of solutions, regardless of variations in model parameters. A dynamical analysis is performed to identify the local stability properties of the viral clearance steady state. This analysis illustrates how chronically infected macrophages can explain the progression to AIDS and provoke viral explosion, while previous models do not. We further demonstrate that the infected T-cell population, even if not responsible for the majority of new infections that lead to viral explosion, may contribute significantly to the transition amongst the three stages of infection. Moreover, we explore the implications of the model for the administration of antiretroviral therapy (ART) and provide quantitative estimates that emphasize the time sensitive nature of treatment initiation and the level of drug efficacy. Finally, we study the effects of treatment interruption on the disease dynamics predicted by the model and elucidate the influence of both interruption time and duration.

Keywords HIV · Three-stage · Viral reservoir · ART · Treatment interruption

Mathematics Subject Classification 92-10 · 92C60 · 92D25 · 92-08

The second author was supported by the US National Science Foundation under awards DMS-1911145 and DMS-2107938.

✉ Stephen Pankavich
pankavic@mines.edu

[1] Department of Applied Mathematics and Statistics, Colorado School of Mines, Golden, CO 80403, USA

Published online: 28 February 2024

1 Introduction

Since the emergence of the Acquired Immunodeficiency Syndrome (AIDS) epidemic within the United States during the early 1980s and the discovery of its pathogenic agent, the human immunodeficiency virus (HIV), the deleterious effects of HIV infection on the human immune system have been extensively studied. The virus is known to infect an essential component of the immune system, $CD4^+$ T cells, ultimately leading, without treatment, to patient death caused by opportunistic infection. According to the World Health Organization, there were approximately 39 million people living with HIV as of 2022 (World Health Organization 2023). Due to the continued global impact of the disease, medical researchers maintain a heightened interest in the study of HIV infection dynamics, including mechanisms that affect the progression of the disease, creation of new antiretroviral treatments, and the possibility of vaccine development.

The mathematical and computational modeling of in-host HIV dynamics has gained a great deal of attention in recent years and become a critical tool to medical researchers battling the progression of the disease. A variety of models, generally consisting of systems of nonlinear differential equations, have been developed to describe the dynamical behavior of HIV within an infected host (Callaway and Perelson 2002; De Boer et al. 2010; Kirschner 1996; Jones et al. 2014; Pankavich 2016; Perelson and Nelson 1999; Nowak and May 2000). Often these investigations seek to identify basic relationships between $CD4^+$ T-cells, their infected counterparts, and the viral load (Jones et al. 2014; Kirschner 1996; Nowak and May 2000; Pankavich and Parkinson 2016), in addition to the infection of secondary target populations and the response of the immune system via cytotoxic T-lymphocytes (Hadjiandreou et al. 2007; Hogue and Bajaria 2008; Kirschner and Perelson 1995). Such models have accurately described the acute stage (during initial or primary infection) and the chronic phase (Nowak and May 2000; Kirschner 1996; Callaway and Perelson 2002), but until recently, none were able to simultaneously represent the final stage of infection, in which the disease process transitions into the development of AIDS. In general, new predictive models, and an understanding of their behavior, play a central role and are continually needed to both advance our understanding of HIV disease dynamics and study the impact of treatment strategies.

During the acute infection period of the disease, which typically last for a few weeks to a few months, an infected individual experiences flu-like symptoms, including fever, sore throat, swelling of glands, rash, and fatigue. Accordingly, a precipitous drop occurs within the concentration of an individual's circulating $CD4^+$ T-cells, as does an exponential increase in the level of free virions. After the conclusion of this phase, the aforementioned symptoms cease, and the infected individual enters the chronic, or latent, infection phase, during which a long asymptomatic period occurs. T-cell levels return to a magnitude similar to the baseline values expected in a healthy individual, while the viral load decreases dramatically. However, HIV continues to infect new cells and actively uses immune cells, including $CD4^+$ and $CD8^+$ T-cells, B-cells, and macrophages, to replicate. Over long time periods, the T-cell count degrades substantially as the viral load continues to increase. This second period of the disease process has been observed to last anywhere from 2 to 20 years with most patients experiencing

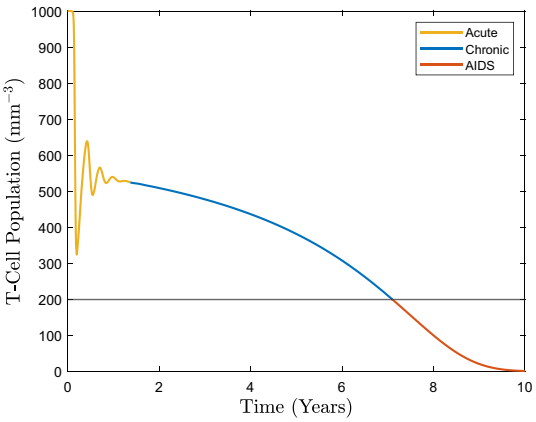

Fig. 1 T-cell Population vs time, depicting the three-stage representation of HIV disease pathogenesis. A measured T-cell count of 200 cells/mm^3 or below (straight line) represents the clinical definition of AIDS

an asymptomatic period between 7 and 10 years, on average (Hernandez-Vargas and Middleton 2013). Finally, as the viral load slowly rises over this period of years, the T-cell count continues to decrease until it reaches a level of 200 cells/mm^3, representing the onset of AIDS. The continuing low level of T-cells renders the immune system of an HIV-positive individual unable to identify and defend itself against opportunistic infection, which without the benefit of drug therapy, ultimately proves fatal. As an understanding of the transition to this last stage is crucial to developing treatment strategies and inhibiting the advancement of AIDS, a model that simultaneously describes all three stages is imperative to battling this now decades-long worldwide epidemic. Of course, a mathematical model that can realistically simulate each phase of disease progression is necessary in order study infection dynamics over long time period (Fig. 1). Hence, such studies were not possible prior to the development of a three-stage model.

Mathematical modeling can also be used to inform, analyze, and predict outcomes of long-term treatment options for HIV-infected individuals. In order to be viable for such purposes, though, they must (i) be capable of both explaining and reproducing clinical data, (ii) provide biologically-relevant reasoning for their formulation, (iii) feature robust control relative to parameter variations that are inevitably present amongst susceptible individuals, and (iv) allow for realistic implementations of treatment strategies. Thus, in addition to describing the entire time course of the HIV disease process, an informative mathematical model must also feature parameters that do not change wildly over time. As far as we are aware, Hadjiandreou et al. (2007) proposed the first differential equations model with the ability to represent all three stages of infection without the use of time-dependent parameters. Numerical results therein demonstrate that macrophages, which may act as long-term reservoirs, can play an important role in the final stages of the disease process. However, simulations of the model in Hadjiandreou et al. (2007) exhibit great sensitivity to parameter variations. In particular, small changes on the order of 3% of nominal values can reduce the standard time course to AIDS from 10 years to just a single year, or perhaps cause it to disappear entirely (Hernandez-Vargas and Middleton 2013). A refined model of the three-stage dynamics of HIV infection, which corrected the unusual sensitivity of the T-cell count with

respect to parameters, was developed in Hernandez-Vargas and Middleton (2013) via a system of five nonlinear differential equations. Further, modifications of this model have been more recently used (Haering et al. 2014; Hernandez-Vargas et al. 2014) in tandem with methods of control theory and Monte Carlo simulation to study antiretroviral treatment strategies that combat the effects of drug-resistant viral mutation to the onset of AIDS. Unfortunately, many of the properties of the original model, including the behavior of solutions, the stability properties of steady states, the parameters of greatest influence on the development of AIDS, and the quantitative impact of antiretroviral therapy (ART) and treatment interruption, have yet to be elucidated. Such analyses represent the key contributions of the current paper.

Modern mathematical approaches to studying in-host disease dynamics often focus on differentiating the behavior of a dynamical model amongst one or more infective and disease-free steady states and then determining the parameters that most greatly influence the stability properties of these states. However, as HIV has been shown to be completely resistant to achieving clearance of the disease, due to the repopulation of virions from viral reservoirs, one cannot expect the disease-free steady state to be reached by biologically-relevant parameter regimes. One significant obstacle in clearing persistent viral infection from individuals is the appearance of latently infected viral reservoirs (Pankavich 2016). Latent HIV often emerges with recrudescence as a productive infection later in disease progression and provides a source for the emergence of resistant strains of the virus. It is widely recognized that macrophages represent a latently infected viral reservoir and are a significant and critical HIV target cell *in vivo* (Hernandez-Vargas and Middleton 2013; Orenstein 2001; Brown et al. 2006). This class of white blood cells can be divided into multiple subsets of macrophage-like cells, all of which are susceptible to HIV infection, including dendritic cells, Langerhans cells, alveolar macrophages, mucosal macrophages, and microglial cells (Gavegnano and Schinazi 2009). A model that incorporates the effects of such secondary target populations, like that of Hernandez-Vargas and Middleton (2013), is necessary to obtain a full, three-stage description of the disease process. Thus, a different approach, i.e. one that does not merely focus on the stability of a disease-free steady state, is needed to study the complete time course of the disease.

One approach is to consider treatment strategies that extend the chronic phase of the disease to suitably long time periods, perhaps many decades or longer. In this way, an infected patient will never experience the transition to AIDS during a realistic lifetime, and thus will not become immunocompromised or susceptible to opportunistic infection. In a later section, we take this approach from a computational perspective in an effort to determine the parameters that most influence the time to the transition from the chronic phase to AIDS. Within the next section, however, we first focus on formulating and validating the proposed model, providing biologically relevant ranges for parameter values, performing a basic sensitivity analysis, and discussing the inherent mathematical properties of the model.

2 Model formulation & properties

We begin by presenting the model of Hernandez-Vargas and Middleton (2013) and describing its formulation. The system of five nonlinear ODEs is given by

$$\begin{cases} \dot{T} = s_T + \dfrac{\rho_T V}{c_T + V} T - k_T T V - \delta_T T \\ \dot{T}^* = k_T T V - \delta_{T^*} T^* \\ \dot{M} = s_M + \dfrac{\rho_M V}{c_M + V} M - k_M M V - \delta_M M \\ \dot{M}^* = k_M M V - \delta_{M^*} M^* \\ \dot{V} = p_T T^* + p_M M^* - \delta_V V \end{cases} \tag{1}$$

with initial conditions $T(0), T^*(0), M(0), M^*(0), V(0) \geq 0$. Here, $T(t)$ represents the density of uninfected CD4$^+$ T-cells and $T^*(t)$ is the density of infected CD4$^+$ T-cells. Similarly, $M(t)$ is the density of uninfected macrophages, while $M^*(t)$ represents the density of infected macrophages, and $V(t)$ is the density of free, productively infectious HIV virions.

The model is comprised of a variety of biological processes. First is the natural generation of new T-cells and macrophages from the thymus and bone marrow at constant rates, namely $s_T = 10$ cells/mm^3 day and $s_M = 0.15$ cells/mm^3 day, respectively (Kirschner and Perelson 1995; Perelson and Nelson 1999). Such mechanisms are not the only manner in which the T-cell and macrophage populations may increase over time, as the appearance of HIV triggers the further proliferation of immune cells. In particular, the antigen-stimulated homeostatic proliferation of T-cells and macrophages is modeled by Michaelis-Menten dynamics that are limited by the viral load. Within the T-cell evolution, this term appears in the form $\frac{\rho_T V}{c_T + V} T$. Here and in the analogous macrophage term, ρ_T and ρ_M are the maximum growth rates, while c_T and c_M are the half-velocity constants of growth. The behavior of this nonlinear term is limited by the growth and decay of the virus population. More specifically, the function $F(V) = \frac{\rho V}{c+V}$ satisfies $F(0) = 0$, $F'(V) > 0$, and $\lim_{V \to \infty} F(V) = \rho$. Hence, when no virions are present in the system, this term vanishes, as an immune response is unecessary in the absence of virions. Contrastingly, as the virus population grows large, the immune system replenishes the T-cell and macrophage populations so as to balance their depletion from viral infection, and this occurs at a growing rate whose maximal impact is ρ_T and ρ_M, respectively. Values of the proliferation parameters were obtained by simulating disease trajectories in comparison to clinically observed data (cf. Hernandez-Vargas and Middleton 2013).

Next, the infection process is modeled in a standard manner amongst in-host viral models. Though HIV can infect a variety of cell types, we focus on the impact to activated CD4$^+$ T-cells and macrophages via a bilinear infection term, for instance $k_T T V$ within the T-cell population evolution. Once T-cells or macrophages become infected, they change compartments, and hence this term decreases the T and M populations and boosts the T^* and M^* populations, as well. The parameter k_T is

Table 1 Parameter values and simulation ranges for (1)

Parameter	Nominal value	Range (10% Variation)	Units
s_T	10	9–11	cells mm^{-3} days^{-1}
s_M	0.15	0.135–0.165	cells mm^{-3} days^{-1}
k_T	4.57×10^{-5}	4.11×10^{-5}–5.02×10^{-5}	mm^3 days^{-1} copies^{-1}
k_M	4.33×10^{-8}	3.90×10^{-8}–4.76×10^{-8}	mm^3 days^{-1} copies^{-1}
p_T	38	34.2–41.8	copies cells^{-1} days^{-1}
p_M	35	31.5 –38.5	copies cells^{-1} days^{-1}
δ_T	0.01	0.009–0.011	days^{-1}
δ_{T^*}	0.4	0.36–0.44	days^{-1}
δ_M	1×10^{-3}	9×10^{-4}–1.1×10^{-3}	days^{-1}
δ_{M^*}	1×10^{-3}	9×10^{-4}–1.1×10^{-3}	days^{-1}
δ_V	2.4	2.16–2.64	days^{-1}
ρ_T	0.01	0.009–0.011	days^{-1}
ρ_M	0.003	0.0027–0.0033	days^{-1}
c_T	300	270–330	copies mm^{-3}
c_M	220	198–242	copies mm^{-3}

merely the rate at which free virions infect T-cells, with an analogous definition for k_M.

As activated T-cells and macrophages are infected, they begin to produce virions. We model viral production and proliferation using terms that are proportionate to the current size of the infected T-cell and infected macrophage populations. In this way, the amount of virus produced by infected T-cells and macrophages is given by $p_T T^*$ and $p_M M^*$, respectively, where p_T and p_M are the individual rates of production per unit time. As before, the range of values of these rates are taken from Hernandez-Vargas and Middleton (2013).

Finally, both cells and virions possess a finite lifespan. Thus, we model the natural death of each population as proportionate to their current values, leading to the exponential time decay of these quantities in the absence of other biological mechanisms. The corresponding constants δ_T, δ_{T^*}, δ_M, δ_{M^*}, and δ_V, all represent the natural death rate of these respective populations. All nominal values (and ranges of their fluctuation) for the aforementioned constants are provided within Table 1.

Throughout the paper, the values of initial conditions found in Hernandez-Vargas and Middleton (2013) are used for computational simulations. In particular, the initial density of T-cells is fixed to be $T(0) = 10^3$ cells/mm^3, the initial macrophage density is $M(0) = 150$ cells/mm^3, and the initial viral concentration is $V(0) = 10$ copies/ml. The densities of infected T-cells and macrophages are initialized to zero so that $T^*(0) = M^*(0) = 0$. We note that throughout the paper all simulations are conducted using MATLAB's `ode23s` ODE solver with the aforementioned parameter values and initial conditions. A representative simulation using these quantities is provided within Figs. 1 and 2.

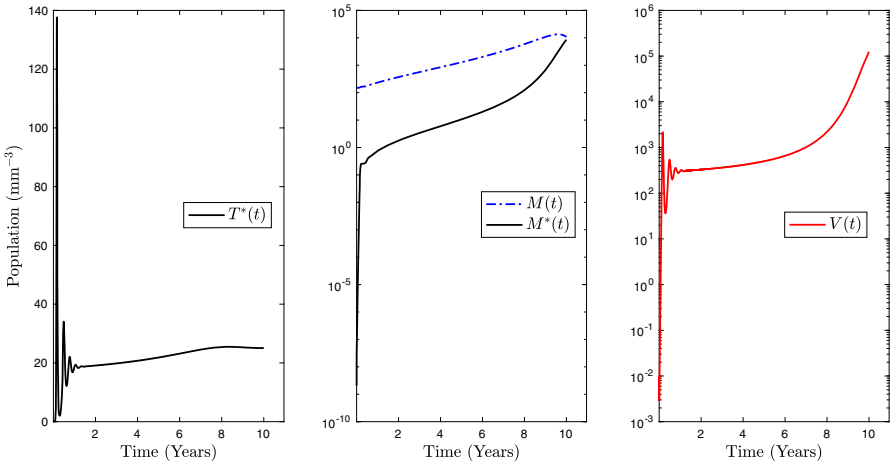

Fig. 2 Graphs of the infected T-cell $T^*(t)$, macrophage $M(t)$, infected macrophage $M^*(t)$, and virion $V(t)$ populations vs time using standard parameter values. The last three populations are plotted on a log-scale along the vertical axis

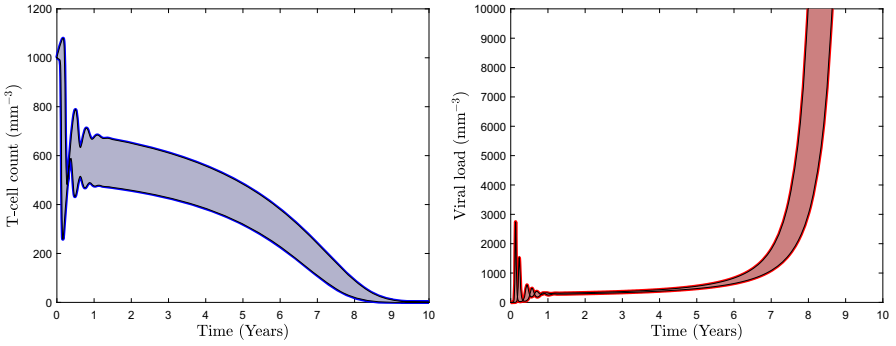

Fig. 3 Sensitivity Analysis with 10% variation in all parameter values: T-cell count (left) and viral load (right). Envelopes represent changes over a sample of size $N = 1,000$ with uniformly distributed parameter variations

Upon setting baseline values of parameters, we performed an initial "all-at-once" sensitivity analysis, allowing parameters to vary by up to 10% above or below their baseline values. Subsequent T-cell and viral time courses are shown in Fig. 3 and display very minor fluctuations over long time periods. Thus, unlike the proposed three-stage model of Hadjiandreou et al. (2007), the system (1) is quite robust with respect to parameter variations. Another issue appearing within the earlier model of Hadjiandreou et al. (2007) is that solutions may become negative at some finite time. Of course, each of these quantities (e.g., the T-cell count and viral load) lose biological significance in such a scenario, and this may invalidate the relevance of the previous model, even near baseline parameter values. In contrast, we show that the positivity (or nonnegativity) of (1) is necessarily preserved in time. Said another way, the density of the T-cell, macrophage, and virion populations cannot become negative at a finite

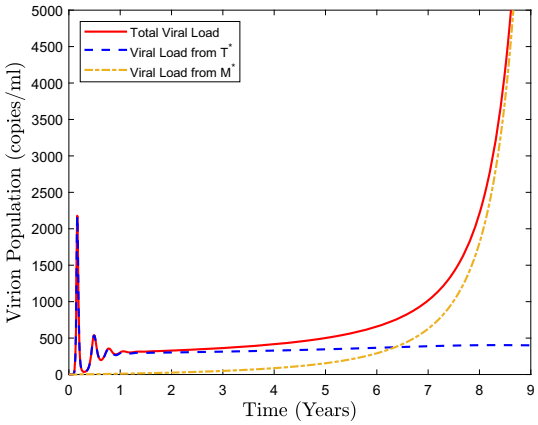

Fig. 4 Multiscale dependence of viral load on the generation of new virions via infected T-cells and infected macrophages

time, though they may vanish in the asymptotic limit as $t \to \infty$. This is displayed by the following theorem:

Theorem 1 *(Positivity) Assume the initial conditions satisfy* $T(0), M(0), V(0) > 0$ *and* $T^*(0), M^*(0) \geq 0$. *Then, these properties are maintained so that* $T(t), M(t), V(t) > 0$ *and* $T^*(t), M^*(t) \geq 0$ *for all* $t \geq 0$. *These quantities also remain bounded on* $[0, \tilde{T}]$ *for any* $\tilde{T} > 0$.

For the sake of continuity, the proof is postponed to Appendix 1. As discussed in the introduction, another crucial property of the model is its multiple time scale evolution and dependence upon a secondary population that is susceptible to HIV infection, namely macrophages. Performing a simulation of (1) with baseline parameter values, one can precisely track the new virions that are generated over time by infected T-cells and infected macrophages, respectively. To accomplish this, the viral load is decomposed into

$$V(t) = V_{T^*}(t) + V_{M^*}(t)$$

where $V_{T^*}(t)$ represents the new virions produced by infected T-cells, satisfying

$$\dot{V}_{T^*} = p_T T^* - \delta_V V_{T^*},$$

while $V_{M^*}(t)$ represents the new virions produced by infected macrophages and satisfies

$$\dot{V}_{M^*} = p_M M^* - \delta_V V_{M^*}.$$

The sum of these factors then provides the complete behavior of the total virus population as given in (1). Figure 4 demonstrates this decomposition for baseline parameter values. Notice that the behavior of the virus population is dictated by the infected T-cell population for the first 1-4 years, after which, infected macrophages become the dominant viral production mechanism. In this way, the infection of T-cells determines

the response of the system during the acute stage, while a slow transition occurs during the chronic stage, and the continuing infection of macrophages drives the system to viral explosion and the onset of AIDS. We will revisit the influence of infected macrophages on the development of AIDS in later sections as it will significantly impact outcomes for patients who are undergoing ART.

With some basic properties of (1) established, we turn our attention to an introductory dynamical analysis of the system, in order to identify any infection-free steady states and determine their associated stability properties. Classically, studying such phenomena will provide information concerning the parameters that promote and inhibit viral clearance or proliferation, respectively.

3 Equilibria & stability analysis

The main focus of this section is to apply traditional tools of mathematical analysis to discover the potential dynamical states of the system and deduce conditions on parameters that imply the stability or instability of these states. We first determine all relevant steady state solutions of the model and perform a stability analysis to gauge their dynamical properties.

Theorem 2 *(Steady States) The system (1) has exactly one non-infected steady state, given by*

$$E_{NI} = \left(\frac{s_T}{\delta_T}, 0, \frac{s_M}{\delta_M}, 0, 0 \right).$$

Furthermore, (1) possesses as many as four distinct infected steady states E_I, which are determined by the positive solutions of a quartic polynomial - see (4) in Appendix 1.

As before, we postpone the proof of Theorem 2 to Appendix 1 for continuity. Furthermore, simulations conducted with up to a 10% variation in parameters from their baseline values show that the steady state equations associated to (1) can, in fact, attain four distinct positive solutions. Hence, the existence of multiple biologically-relevant steady states displays the inherent complexity of the model, and an explicit representation of these steady states in terms of parameter values is not easily obtained. Next, we explore the stability properties of E_{NI}.

Theorem 3 *(*Stability & Instability) Let

$$R_T = \frac{p_T k_T s_T}{\delta_T \delta_{T^*} \delta_V}$$

and

$$R_M = \frac{p_M k_M s_M}{\delta_M \delta_{M^*} \delta_V}$$

represent basic reproduction numbers corresponding to the T-cell and macrophage populations, respectively. Then, E_{NI} is locally asymptotically stable if

$$R_T + R_M < 1$$

and unstable if

$$R_T + R_M > 1.$$

To streamline the exposition, we also postpone the proof of this result to Appendix 1. Here, the basic reproduction number associated to T-cell infection is denoted R_T, while the analogous reproduction number for macrophage infection is denoted by R_M. These represent the average number of secondary infections produced by a single new T-cell or macrophage infection, respectively. Using baseline parameter values, the associated reproduction numbers are

$$R_T = 1.809 \quad \text{and} \quad R_M = 0.09$$

and even a 40% change in parameters cannot reduce the sum $R_M + R_T$ below one. Further, notice that $R_T \gg R_M$, and this remains true even if one accounts for variability in parameter estimates. Therefore, while the infection of macrophages is driving the transition to AIDS, reducing the reproduction number R_M that stems from the parameters associated to macrophage infection will not result in the stability of the viral clearance state. Indeed, the value of R_T remains unchanged even if the infection rate of macrophages is drastically reduced. Though infected T-cells are typically seen as the primary driver of infection, the infected macrophage population is responsible for producing the overwhelming majority of new virions during the transition to AIDS. Indeed, Fig. 4 demonstrates that the infected macrophage population induces the rapid growth of the viral load. In this direction, if one takes $p_M = 0$ within the model, then the M^* population decouples from the remaining differential equations, and the dynamics reduce to a three-dimensional system for $T(t)$, $T^*(t)$, and $V(t)$, which was studied in detail within Pankavich et al. (2020). Fixing all other parameters to baseline values results in the development of a persistent infection, as expected from Theorem 3, but neither viral explosion nor a steady decrease in the T-cell count occurs to drive the system to AIDS as depicted in Fig. 5. Similarly, if one takes $p_T = 0$ and fixes all other parameter values to baseline, the T-cell evolution is decoupled from the system, and the primary infection mechanism is lost. This induces an immediate and rapid decline of the initial viral load (see Fig. 5) and eliminates the pool of virions required to generate the acute and chronic phases, thereby removing the initial driving force that guarantees a suitably large viral load to sustain the persistent infection of macrophages and lead to viral explosion. Hence, it appears that these two infection processes (via T-cells and macrophages) must work in tandem to generate all three stages of the disease process, and a suitable threshold of virions is needed during the chronic phase in order for the infected macrophages to drive the system beyond a viral persistence equilibrium and into the final, viral explosion stage.

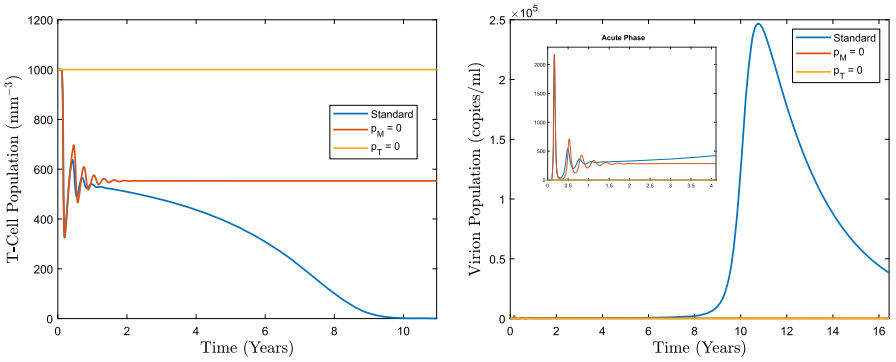

(a) T-cell Population **(b)** Virion Population

Fig. 5 Plots of T-cell and virion populations comparing baseline parameter simulations to those in which $p_M = 0$ and $p_T = 0$, respectively. When $p_M = 0$, E_{NI} is unstable, and the T-cell and virion populations converge to a locally stable infectious steady state E_I, namely with $T(t) \to 552$ and $V(t) \to 283$, as $t \to \infty$. Furthermore when $p_T = 0$, the non-infectious steady state E_{NI} is stable with $T(t) \to 1000$ and $V(t) \to 0$ as $t \to \infty$

We further note that the reduced system of differential equations in Pankavich et al. (2020) has already been shown to display significantly complex behavior, including two stable, persistently-infected steady states, regions of infected bistability, and the appearance of both limit cycles and a Hopf bifurcation. As $M(t) \ll T(t)$ during the acute phase and the majority of the chronic phase, the short-time dynamical picture of (1) is quite similar. However, for large times a full dynamical understanding of (1) becomes significantly more complex.

While mathematical analysis can provide information regarding the large time asymptotic behavior of in-host models like (1), the current clinical focus on combating HIV-1 infection centers on prolonging the chronic phase of the disease indefinitely via viral suppression, not the total eradication of the disease, which is intractable due to numerous viral reservoirs. Therefore, in the next section, we employ a computational approach to identify parameters that most greatly contribute to the extension of the chronic phase beyond the standard time period expected for the transition to AIDS.

4 Transition from chronic infection to AIDS

As demonstrated within the previous section, only a subset of the parameters, namely those appearing within R_T and R_M, regulate the stability or instability of the non-infected state E_{NI}. However, as we'll show, other parameters within the three-stage model can still drastically influence the behavior of the T-cell count and viral load throughout the time course of the disease.

Due to the persistence of viral reservoirs, modern treatment strategies do not attempt to completely eradicate HIV within an infected patient, but instead focus on extending the chronic phase of the disease, thereby prolonging the onset of AIDS for as long as possible. For this reason, we will turn our attention to studying and comparing

functions that may characterize the duration of the chronic phase. In particular, let

$$p = [s_T, s_M, \ldots, c_T, c_M] \in \mathbb{R}^{15}$$

represent the vector of parameter values in the system (1) ordered by their appearance in Table 1. Using this notation, we represent the T-cell count after $t > 0$ years by $\mathcal{T}(t; p)$ in order to demonstrate its dependence upon the high-dimensional set of parameters. Next, we similarly formulate the parameter-dependent "Time to AIDS" function $\mathcal{F} : \mathbb{R}^{15} \to \mathbb{R}$ defined by

$$\mathcal{F}(p) = \max \{t \geq 0 : \mathcal{T}(t; p) > 200\}.$$

This quantity represents the maximal time at which an infected individual's T-cell count remains above the clinically-defined AIDS threshold of 200 cells per mm^3, and thus for any set of parameters, outputs the time until the onset of AIDS.

Because analytical methods for understanding the transition from the chronic stage to the emergence of AIDS are limited, we take a computational approach. In particular, we use an active subspace decomposition to determine the parameters of greatest influence on $\mathcal{F}(p)$ and $\mathcal{T}(t; p)$ for fixed $t > 0$, which will further allow us to construct reduced-order approximations of these functions. For completeness, we outline the basics of an active subspace decomposition in Appendix 1. The high dimensional nature of the domains of $\mathcal{T}(t; p)$ and $\mathcal{F}(p)$ makes visualization particularly challenging. Hence, we will project the values of these functions onto the single direction in $\mathbb{R}^{15}$ along which they vary the most.

In this vein, the active subspace decomposition allows us to determine the parameters that most greatly influence the values of these functions of p. In particular, Fig. 6(a) demonstrates that three parameters (due to the magnitude of their weight vector entries) primarily influence $\mathcal{T}(5; p)$, representing the T-cell count after 5 years, namely (i) p_T, the production rate of virions from infected T-cells (parameter 5), (ii) δ_{T^*}, the clearance rate of infected T-cells (parameter 8), and (iii) δ_V, the virion clearance rate (parameter 11). These quantities are generally expected to influence the T-cell count at any particular time, especially considering their appearance within the associated basic reproduction number R_T and the stability properties of the viral clearance equilibrium E_{NI} demonstrated by Theorem 3. While they also affect $\mathcal{T}(10; p)$ and $\mathcal{F}(p)$, as seen in Figs. 6(b) and 6(c), there is another parameter that drastically influences an infected individual's time until the onset of AIDS, namely ρ_M, the rate of macrophage recruitment due to the presence of virions (parameter 13). This is indicative of macrophage infection driving the growth of the virus population in the later stages of the disease process, as an increased macrophage population presents a greater potential for viral reservoirs. We note that ρ_M does not significantly impact $\mathcal{T}(5; p)$, likely because the disease is still experiencing the chronic phase wherein the virions produced by infected T-cells are the main engine of viral production. In contrast, after 10 years the virions produced by infected macrophages begin driving the system to AIDS. However, notice that ρ_M does not appear within R_T or R_M, and thus does not influence the qualitative behavior of the disease-free equilibrium in any manner. That being said, this parameter clearly has a quantitative influence on the rate at which solutions may tend to an infected equilibrium state or induce

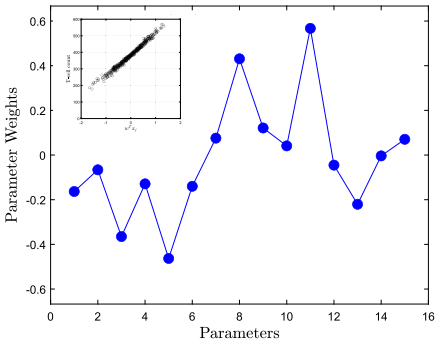

(a) Active Subspace decomposition for $\mathcal{T}(5; p)$

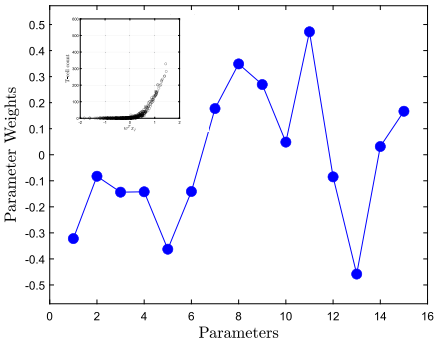

(b) Active Subspace decomposition for $\mathcal{T}(10; p)$

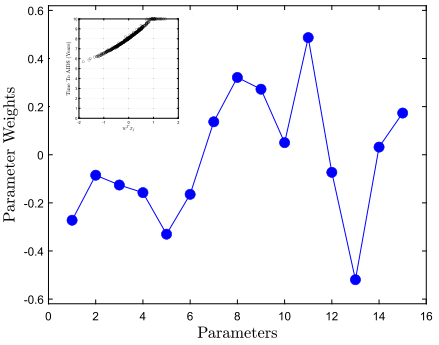

(c) Active Subspace decomposition for $\mathcal{F}(p)$

Fig. 6 Parameter weights and sufficient summary plots (inset) for $\mathcal{T}(5;\ p)$, $\mathcal{T}(10;\ p)$ and $\mathcal{F}(p)$. Parameters along the horizontal axis are labelled in order as presented within Table 1

viral explosion. Indeed, if the value of ρ_M is increased, then more macrophages are recruited to fight the persistent infection, and thus, additional target cells are available for HIV to infect and spread the infection. The values of $\mathcal{T}(t;\ p)$ at longer times t were further explored to evaluate variables of greatest influence, and similar results emerged for $\mathcal{T}(15;\ p)$ and $\mathcal{T}(20;\ p)$ as did for $\mathcal{T}(10;\ p)$. Finally, Fig. 6 shows that the weight vector decompositions for $\mathcal{T}(10;\ p)$ and $\mathcal{F}(p)$ are nearly identical, implying that the same parameters that determine an individual's T-cell count after 10 years further indicate the time until the onset of AIDS.

Inset within Fig. 6 are sufficient summary plots of the respective variable of interest, i.e., $\mathcal{T}(5;\ p)$, $\mathcal{T}(10;\ p)$, or $\mathcal{F}(p)$, as functions of the first active variable, namely the linear combination of parameters with the weight vectors shown in Fig. 6 serving as the coefficients (or coordinates) of these parameters. As each weight vector represents the direction of greatest influence of parameters on the respective output quantity, e.g. $\mathcal{F}(p)$, the sufficient summary plot constitutes the projection of the output quantity onto the dominant active subspace, namely the direction described by the weight vector. Notice that the output quantities are increasing as functions of the first active variable. Hence, those parameters with positive weight vector entries promote an increase in (or positive correlation with) the output variable, while those with negative weight vector

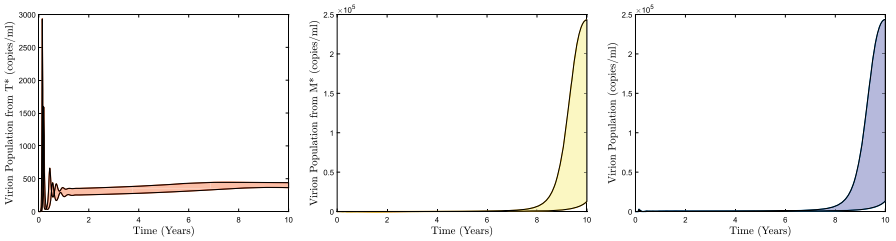

(a) New virions produced from infected T-cells $V_{T^*}(t)$ **(b)** New virions produced from infected macrophages $V_{M^*}(t)$ **(c)** Total number of virions $V(t)$

Fig. 7 Decomposition of viral population; shading represents a 10% variation in δ_V. These results are similar for variations in δ_{T*}

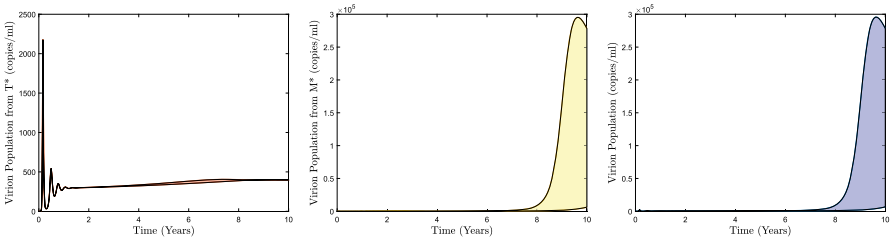

(a) New virions produced from infected T-cells $V_{T^*}(t)$ **(b)** New virions produced from infected macrophages $V_{M^*}(t)$ **(c)** Total number of virions $V(t)$

Fig. 8 Decomposition of viral population; shading represents a 10% variation in ρ_M

entries promote a decrease in (or negative correlation with) the output variable. For instance, for each of the output variables Fig. 6 demonstrates that ρ_M (parameter 13) is negatively correlated, while the other parameters of greatest influence, i.e. δ_V, δ_{T^*}, and p_T, are all positively correlated with the output. Furthermore, the sufficient summary plots provide details about the approximate behavior of these output quantities. In particular, the inset of Fig. 6(a) shows that after 5 years very few of the randomly-sampled time courses produce T-cell counts below the clinical threshold for AIDS, while the inset of Fig. 6(b) demonstrates the opposite, namely that the overwhelming majority of randomly-sampled parameter sets lead to the onset of AIDS within 10 years. Finally, the inset of Fig. 6(c) provides direct estimates on the time (in years) until the progression to AIDS, with a generally linear distribution ranging between 5 and 10 years.

Now that the parameters of greatest influence on T-cell counts have been determined, we may further study how variations in the values of these quantities affect the viral load over its entire time course. To begin, we perturb δ_V by up to a 10% variation from its baseline value and study the corresponding changes in (i) the virions produced by infected T-cells $V_{T^*}(t)$, (ii) the virions produced by infected macrophages $V_{M^*}(t)$, and (iii) the total number of virions $V(t)$ over time. As seen in Fig. 7, δ_V exerts a greater influence upon viral production by infected macrophages than it does for virions arising from infected T-cells. Figure 8 shows similar behavior for up to a 10% variation from baseline values of ρ_M, and the effect on $V_{T^*}(t)$ is essentially negligible. Hence, these

parameters modify the time until the transition to AIDS mainly by influencing the growth rate of virions produced by infected macrophages.

Though variations in the values of ρ_M, δ_V, p_T, and δ_{T^*} can lead to significantly longer times until the onset of AIDS, the values of most of these parameters are not actually determined by external factors. However, the parameter p_T can be altered by the implementation of antiretroviral therapy. Thus, in the next section, we implement a time-dependent ART treatment strategy to understand how drug therapy can be applied to prolong an individual's progression to the final stage of the disease.

5 Administration of ART

In order to study the model's capability to explain the effect of realistic treatment strategies, we introduce the administration of ART within the system. A variety of previous studies (Pankavich and Shutt 2015; Rong et al. 2007; Xia 2007) have attempted to understand the influence of antiretroviral drugs by using constant drug efficacies, which tacitly assumes that an infected individual begins ART at the time of infection. Doing so in the model (1) would merely utilize the result of Theorem 3 and alter the parameters k_T and p_T. In particular, upon denoting the drug efficacy by $\epsilon \in [0, 1]$, we would rescale parameters by taking

$$k_T^\epsilon = (1-\epsilon)k_T, \qquad p_T^\epsilon = (1-\epsilon)p_T$$

to replace the previous values of these parameters. Here, we assume that ART does not display an appreciable effect on the continued infection of macrophages, as shown in Gavegnano and Schinazi (2009). This alters the corresponding reproduction number so that

$$R_T = \frac{p_T k_T s_T}{\delta_T \delta_{T^*} \delta_V}(1-\epsilon)^2,$$

and a simple calculation demonstrates that, using baseline parameter values, an efficacy of $\epsilon = 0.26$ would be needed in order to drive the system to the infection-free steady state via Theorem 3.

While this can be useful to better understand the dynamics of the model via a reduction in basic reproduction numbers, it is highly unrealistic, as many HIV-positive individuals may not be diagnosed for months, or even years, post-infection. In particular, a few studies (Crepaz et al. 2021; van Sighem et al. 2015) have estimated that the average HIV-infected individual is typically diagnosed around 3 to 3.5 years after initial infection. The Centers for Disease Control have provided similar recent estimates (Centers for Disease Control and Prevention 2019). Thus, HIV-infected individuals often do not begin antiretroviral therapy until well after the acute phase has concluded. Additionally, in the above scenario a 30% constant drug efficacy ($\epsilon = 0.30$) routinely drives the model to the non-infected (viral clearance) steady state even with variation amongst parameters taken into account, while antiretroviral drug efficacy is often significantly greater than this percentage (i.e., closer to 60-90%) Lee et al.

(2014). For these reasons, a time-dependent function is needed to study the long-term effects of ART. Hence, we consider a more realistic implementation consisting of (i) a post-infection but pre-diagnosis period during which antiretroviral therapy is not administered due to the lack of an HIV-positive diagnosis and (ii) a post-diagnosis period during which ART is administered. Of course, the use of a time-dependent parameter generally precludes an analytical approach to studying the influence of treatment, and so we take a purely computational approach. Additionally, though the concentrations of antiretroviral drugs continuously vary due to drug absorption, distribution, and metabolism in the body (Rong et al. 2007), these effects can be averaged to provide a useful understanding of their efficacy. For simplicity, we use a constant impulse function to model the combined administration of ART drugs (e.g., reverse transcriptase inhibitors and either protease or integrase inhibitors, which are typically the constituents of an initial treatment regimen (What to Start 2022)) into a single drug efficacy, though their effects can be separated and more detailed pharmacokinetic models can be used to represent the implementation of ART (Rong et al. 2007). In this way, our approach represents the introduction of a constant efficacy of antiretroviral drugs at a prescribed time.

We assume that the efficacy, denoted by $\epsilon \in [0, 1]$, of the therapeutic regimen remains constant throughout the treatment period and begins at a fixed time $t_\epsilon > 0$. Then, the introduction of ART with these constraints is modeled using a Heaviside function $H(t)$ so that

$$\mathcal{A}(t) = 1 - \epsilon H(t - t_\epsilon)$$

where

$$H(t) = \begin{cases} 0, & \text{for } t < 0 \\ 1, & \text{for } t \geq 0. \end{cases}$$

We note that, while t_ϵ is generally implemented on the timescale of days within this formulation and resulting simulations, we will often provide this value on the scale of years for expositional clarity. As ART disrupts both the viral infection process and the maturation of newly produced virions via a variety of drug classes, for instance entry, reverse transcriptase, integrase, or protease inhibitors, this effect is accounted for by modifying the original model (1) to

$$\begin{cases} \dot{T} = s_T + \dfrac{\rho_T V}{c_T + V} T - \mathcal{A}(t) k_T T V - \delta_T T \\ \dot{T}^* = \mathcal{A}(t) k_T T V - \delta_{T^*} T^* \\ \dot{M} = s_M + \dfrac{\rho_M V}{c_M + V} M - k_M M V - \delta_M M \\ \dot{M}^* = k_M M V - \delta_{M^*} M^* \\ \dot{V} = \mathcal{A}(t) p_T T^* + p_M M^* - \delta_V V. \end{cases} \tag{2}$$

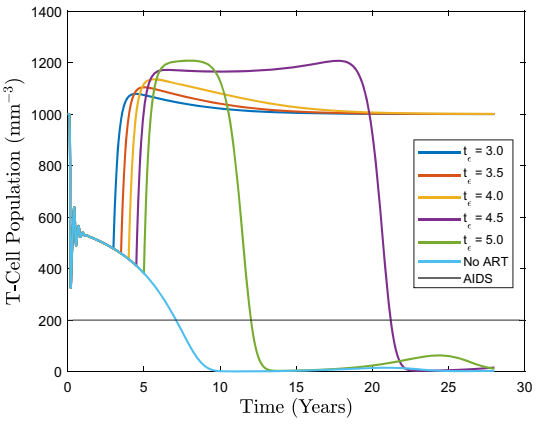

Fig. 9 T-cell population with implementation of ART ($\epsilon = 0.75$) with varied introduction times (in years)

Here, the term $\mathcal{A}(t)k_T T V$ describes a reduction in new T-cell infections due to the implementation of an entry or reverse transcription inhibitor, each of which disrupts the HIV infection process within a healthy T-cell. Similarly, the term $\mathcal{A}(t)\, p_T T^*$ represents a depletion in the production of newly infectious virions due to the suppression of the viral replication and maturation processes post-infection, and thus models the effects of integrase and protease inhibitors. Therefore, the number of infected T-cells and newly-produced virions are significantly reduced by antiretroviral therapy.

As previously mentioned, the infection process for macrophages within (2) is not altered by $\mathcal{A}(t)$. This is because current ART often displays differential antiviral activity in macrophages relative to T-lymphocytes. Though a great deal of effort has been exerted to establish the antiviral activity of many clinically approved antiretroviral therapies in macrophages, a direct link between potential antiviral activity and specific mechanisms responsible for antiviral effects remains incompletely understood (Gavegnano and Schinazi 2009). In particular, recent studies (Gavegnano and Schinazi 2009; Gavegnano et al. 2008; McGee et al. 2006) suggest that ART is significantly less impactful on the macrophage population than within T-cells, and the ability to consistently deliver effective concentrations of drug to macrophages across all organs and tissue compartments is particularly poor. Hence, within the augmented model it is assumed that ART does not inhibit the viral infection or production processes in macrophages.

To describe the effects of ART on the time course of the disease within an HIV-infected individual, simulations were conducted with baseline parameter values given in Table 1 with a total drug efficacy of 75% ($\epsilon = 0.75$) at differing times of ART initiation. Throughout, we consider $t_\epsilon = 3.5$ years to be the average time of treatment initiation (Centers for Disease Control and Prevention 2019). As Fig. 9 displays, the T-cell count post-implementation of ART can vary both widely and in a nonlinear fashion depending upon the time at which an individual first begins treatment. In particular, the introduction of ART at $t_\epsilon = 4.5$ years compared to $t_\epsilon = 5$ years extends the transition to AIDS by approximately 9 years, while earlier implementation - even by an additional six months - can provide significantly improved longevity of the chronic phase, often beyond the expected lifetime of the infected patient. Introduction at later

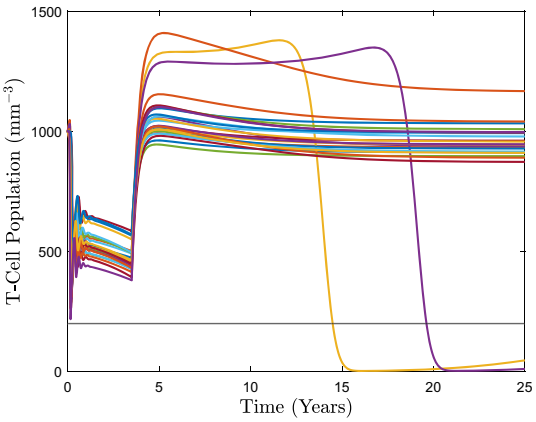

Fig. 10 Sample of 25 random trials with 10% parameter variation and ART introduced at $t_\epsilon = 3.5$ years at an efficacy of $\epsilon = 0.75$

times appreciably blunts the effects of treatment, as the viral load has already begun its increasing trend toward explosion. Thus, as a first major observation, we note that even patients who are continuously treated via antiretroviral therapy may progress to AIDS within a relatively short time period, and the length of time until progression is highly dependent upon both ϵ and t_ϵ.

Though these preliminary simulations clearly display the prolonging benefit of ART, they do not account for fluctuations in parameter values, which represent differences amongst physical characteristics of HIV-infected patients. Hence, to apply ART with parameter variability, simulations with random parameter samples were also conducted. A plot of 25 such random trials allowing for a uniformly-distributed 10% variation in parameter values is provided within Fig. 10. This represents one collection of simulations incorporating ART implementation at $t_\epsilon = 3.5$ years with an efficacy of $\epsilon = 0.75$. Ultimately, a larger simulation of $N = 10,000$ trials with uniformly-distributed 10% parameter variations was conducted, and the response to ART for differing efficacies and administration times was measured. As displayed by Table 2, these simulations show that for a drug efficacy of $\epsilon = 0.75$, reducing the time at which ART is administered from $t_\epsilon = 3.5$ years to $t_\epsilon = 3$ years leads to a 70% reduction in the number of 20-year progressors - from approximately 9.2% to 1.3% of the simulated population. In contrast, if ART is administered later, for instance at $t_\epsilon = 4$ years post-infection rather than $t_\epsilon = 3.5$ years, then the probability that an infected patient progresses to AIDS within 20 years nearly triples (from around 9% to 26%). Similarly, this probability increases to nearly 50% if ART is first implemented at $t_\epsilon = 4.5$ years after initial infection. This analysis extends to other drug efficacies and implementation times, and we have provided results in Table 2, in which the drug efficacies range from $\epsilon = 0.60$ to $\epsilon = 0.85$ and implementation times vary from $t_\epsilon = 2.5$ years to $t_\epsilon = 4.5$ years. We note that the average time to progression (provided by the last row in each block of the table) does not change drastically with respect to differing drug efficacies but is significantly altered by differing implementation times. More specifically, fixing $t_\epsilon = 4.5$ and moving down the last column yields a variation of about 20% in the probability of progression as ϵ is increased, while fixing $\epsilon = 0.6$ and moving across the middle column yields a variation of around 66% in the

probability of progression as t_ϵ is increased. Hence, it appears that the time of ART implementation t_ϵ influences the time until the onset of AIDS more than variations in the drug efficacy ϵ. Furthermore, a decrease in implementation time by six months for any efficacy generally results in an extension of the chronic phase by 1-2 years upon averaging across all populations (i.e., parameters) with a much larger benefit for a single individual. This provides a quantification of the qualitative understanding that medical researchers have understood for quite some time, namely that early administration of ART is critical to prolonging life expectancy for HIV-infected patients and pushing the final stage of the disease process beyond standard human lifespans.

Analogous random simulations were conducted without the implementation of ART in order to provide greater context on the implications of therapy. In particular, $N = 10{,}000$ random trials were performed with a 10% uniformly-distributed variation in parameter values and $\epsilon = 0$. Results of model simulations demonstrate that without ART, HIV-infected patients experienced a 98% probability of progression within 10 years, and this increased to 100% within 15 years. Additionally, the average time to progression amongst untreated individuals is 7.28 years, while the average time to progression when ART is implemented (at time $t_\epsilon = 3.5$ years and an efficacy of $\epsilon = 0.75$—see Table 2) is 14 years, roughly doubling the projected time to the onset of AIDS.

In order to visualize the effects of specific ART combinations on an individual patient (i.e., the same set of parameters), random sets of parameter values from the $10,000$ samples were selected. Both the T-cell and virion populations were plotted with (i) a fixed t_ϵ and varying ϵ, and then (ii) a fixed ϵ and varied t_ϵ as seen in Figs. 11 and 12. Within the latter figure, parameters were selected to demonstrate a worst-case scenario in which all resulting combinations of ART still lead to a progression to AIDS within 20 years. Here, we note that constant variations in either t_ϵ or ϵ can produce a nonlinear effect in the time to the development of AIDS. For instance, Fig. 12(c) shows that implementing ART at $t_\epsilon = 3$ years post-infection instead of $t_\epsilon = 2.5$ years post-infection reduces the length of the chronic phase by approximately 5.5 years, while extending the implementation time by an additional 6 months, moving from $t_\epsilon = 3$ years to $t_\epsilon = 3.5$ years, reduces the chronic phase by only an additional 2.5 years. Hence, as the time of implementation becomes greater, the ability of ART to significantly prolong the transition to AIDS is notably reduced. Similarly, Fig. 11(a) displays the nonlinear response in the drug efficacy, as increasing ϵ from 0.75 to 0.8 extends the chronic phase by 2 years, while further increasing the drug efficacy from 0.8 to 0.85 extends the chronic phase by an additional 4.5 years.

Even after implementing ART, a clear distinction occurs between those HIV-infected patients who progress to AIDS within shorter time frames and those for whom this transition extends beyond the normal human lifespan. In order to better understand the fundamental mechanisms of this dichotomy that may drive the progression to AIDS even in the presence of continuing antiretroviral therapy, we study the same viral decomposition as in Section 2 modified by the introduction of ART. In particular, we write

$$V(t) = V_{T^*}(t) + V_{M^*}(t)$$

Table 2 Probability (in %) of progressing to AIDS. Sample size is $N = 10,000$, and parameters may vary by up to 10% of baseline values. For $t_\epsilon = 2.5$ years and $\epsilon \geq 0.8$, none of the trials progressed to AIDS within a 50 year timespan

Progression Before (years)	$t_\epsilon = 2.5$	$t_\epsilon = 3.0$	$t_\epsilon = 3.5$	$t_\epsilon = 4.0$	$t_\epsilon = 4.5$
$\epsilon = 0.60$					
10	0.11	1.20	6.07	17.13	31.13
15	1.02	6.59	21.44	42.53	60.68
20	1.59	9.13	26.78	49.10	67.68
50	1.88	10.30	28.94	51.52	69.93
Average time	15.44	14.60	13.28	12.16	11.36
$\epsilon = 0.65$					
10	0.01	0.50	3.81	12.76	25.62
15	0.27	3.35	15.10	34.40	54.92
20	0.47	4.84	19.21	40.79	61.82
50	0.55	5.45	20.68	42.79	63.89
Average time	15.73	14.79	13.45	12.45	11.63
$\epsilon = 0.70$					
10	0.00	0.16	2.02	8.94	20.41
15	0.08	1.60	9.24	27.67	47.27
20	0.10	2.34	12.14	33.34	53.94
50	0.13	2.72	13.42	35.45	56.15
Average time	15.65	15.22	13.93	12.83	11.92
$\epsilon = 0.75$					
10	0.00	0.06	1.32	6.01	16.53
15	0.01	0.72	6.89	21.05	41.58
20	0.03	1.28	9.22	26.43	48.62
50	0.04	1.50	10.08	28.14	50.70
Average time	16.65	15.97	14.08	13.07	12.14
$\epsilon = 0.80$					
10	0.00	0.03	0.62	4.22	13.85
15	0.00	0.31	4.15	16.85	37.32
20	0.00	0.64	5.83	21.3	43.55
50	0.00	0.74	6.68	22.95	45.86
Average time	N/A	16.01	14.70	13.41	12.39
$\epsilon = 0.85$					
10	0.00	0.01	0.35	3.42	10.57
15	0.00	0.21	3.20	14.25	33.28
20	0.00	0.38	4.46	18.52	40.38
50	0.00	0.49	5.08	20.12	42.50
Average time	N/A	16.46	14.87	13.68	12.72

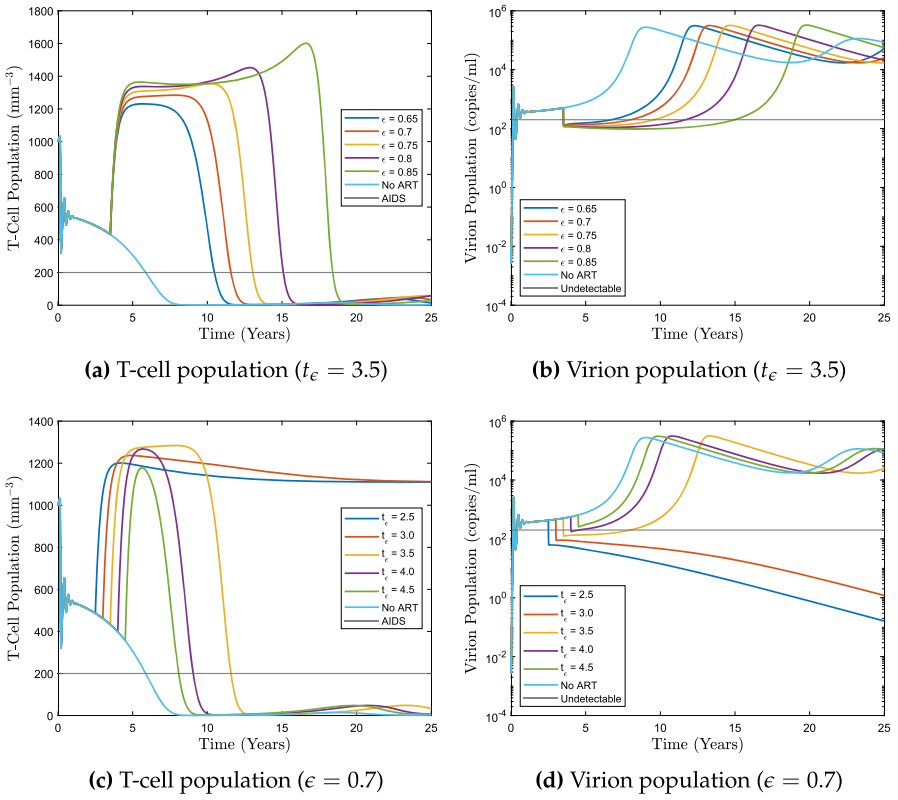

(a) T-cell population ($t_\epsilon = 3.5$)

(b) Virion population ($t_\epsilon = 3.5$)

(c) T-cell population ($\epsilon = 0.7$)

(d) Virion population ($\epsilon = 0.7$)

Fig. 11 Time courses of T-cell and virion populations with respect to fixed implementation times t_ϵ (panels a and b) and fixed efficacies ϵ (panels c and d), respectively. Notice that the virion population initially decreases below the detectable threshold within a few months as routinely observed in a clinical setting (National Institute of Allergy and Infectious Diseases 2020)

where V_{T^*} satisfies

$$\dot{V}_{T^*} = \mathcal{A}(t)\, p_T T^* - \delta_V V_{T^*}$$

and V_{M^*} satisfies

$$\dot{V}_{M^*} = p_M M^* - \delta_V V_{M^*}$$

similar to (1), and simulate the dynamics of (2) while tracking these separate components of $V(t)$. Within these simulations, we fix $\epsilon = 0.5$ and consider differing values of the ART implementation time, namely at $t_\epsilon = 3, 3.5$, and 4 years. The result is that within the simulated viral time course, extremely subtle changes in the value of the viral load at the time of ART implementation, namely $V(t_\epsilon)$, can have a pronounced influence on the transition to AIDS. As shown in Fig. 13, the values of $V(t_\epsilon)$ are not significantly different as t_ϵ is varied, but the outcomes differ dramatically. Indeed, the viral load does not rebound when $t_\epsilon = 3$ with $V(t_\epsilon) = 363$, but experiences viral

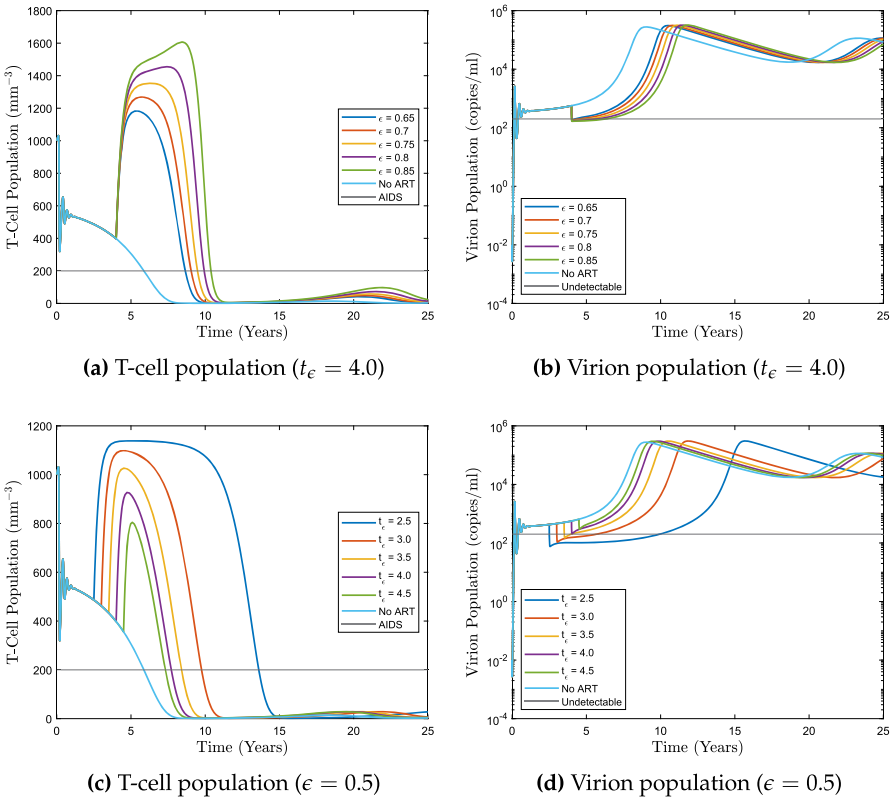

(a) T-cell population ($t_\epsilon = 4.0$)

(b) Virion population ($t_\epsilon = 4.0$)

(c) T-cell population ($\epsilon = 0.5$)

(d) Virion population ($\epsilon = 0.5$)

Fig. 12 Time courses of T-cell and virion populations with respect to fixed implementation times t_ϵ (panels a and b) and fixed efficacies ϵ (panels c and d), respectively

explosion at around 18 years when $t_\epsilon = 3.5$ with $V(t_\epsilon) = 387$ and at around 12 years when $t_\epsilon = 4$ with $V(t_\epsilon) = 416$.

As such minor fluctuations in the viral load induce exceedingly distinct outcomes, we further investigate the detailed role that the size of the macrophage and infected macrophage populations play in this process. In this direction, the percent increase in each of the V, M, and M^* populations was quantified subject to varying ART implementation times and with a uniformly-distributed 10% parameter variation by evaluating the average values of these populations at the implementation time t_ϵ. This metric provides insight into which of these populations plays the largest role in the viral explosion that dominates the third phase of HIV disease progression. As seen by Table 3, the average percent increase of these quantities indicates that, relative to their scale, infected macrophages are most greatly altered by the change in t_ϵ. In fact, the increase in M^* is approximately 1.5 times greater than non-infected macrophages and 4 times that of the virion population, thereby indicating that the increased strength of the infected macrophage population prior to the implementation of antiretroviral therapy is truly driving the distinction between short-term and long-term progression to AIDS. This result further matches the current understanding of the disease process

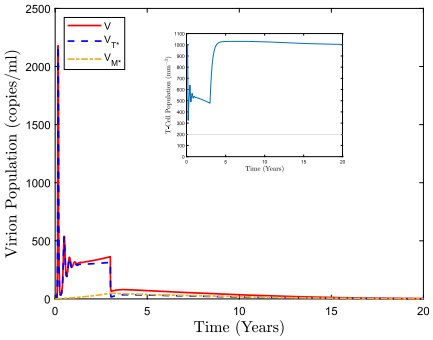

(a) Viral decomposition with ART introduction after 3 years - no progression to AIDS within 100 years

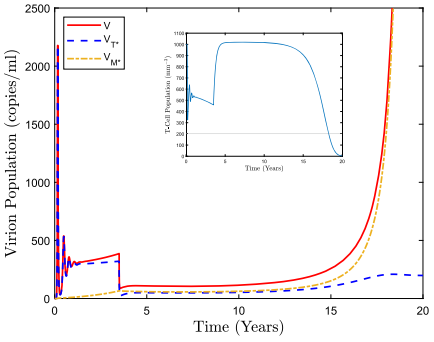

(b) Viral decomposition with ART introduction after 3.5 years - progression to AIDS in 18.5 years

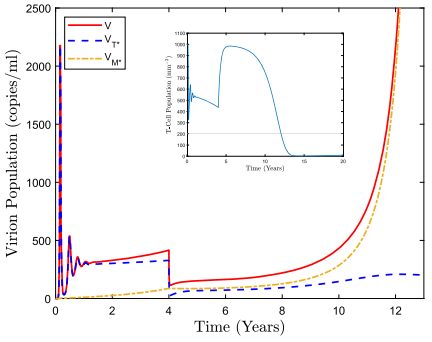

(c) Viral decomposition with ART introduction after 4 years - progression to AIDS in 12 years

Fig. 13 Comparison of viral decomposition (inset: T-cell count) with different time courses for different introduction times of ART, $\epsilon = 0.5$

Table 3 Average relative increase in virion, V, macrophage, M, and infected macrophage, M^* populations generated by changes in time of ART implementation t_ϵ with a uniformly-distributed 10% random parameter variation and 10, 000 trials

Change in t_ϵ	$t_\epsilon = 3 \rightarrow t_\epsilon = 3.5$			$t_\epsilon = 3.5 \rightarrow t_\epsilon = 4$		
Populations	V	M	M^*	V	M	M^*
Average Relative Increase	6.45%	19.73%	27.89%	7.46%	19.63%	27.21%

over long times, as viral reservoirs in myeloid cells are believed to drive progression from the chronic phase to AIDS (Mitchell et al. 2019; Koppensteiner et al. 2012). Thus, we conclude that (i) ART may have a limited ability to sustain long term control of HIV infection due to the impact of viral reservoirs via productively infected macrophages that are generally unaffected by drug therapy, (ii) seemingly negligible differences in the viral load at the time of ART initiation may correspond to significant changes in the relative onset time of AIDS, and (iii) the time of ART implementation is markedly more important than drug efficacy to prolonging the chronic phase of the disease.

6 Interruption of ART

As displayed within the previous section, the influence of ART, and in particular the time at which ART is implemented, is paramount to understanding and predicting the long term outcomes of HIV-infected patients. Another natural question to ask in this direction is how the interruption of ART may further influence treatment outcomes, as breaks in treatment may further expedite the growth of viral reservoirs and lead to an increase in time to progression.

It has been well documented that discontinuation or interruption of antiretroviral therapy can result in viral rebound, immune decompensation, or clinical progression to AIDS (Minority HIV Fund 2022; Lau et al. 2019). In fact, since the halting of the Strategies of Management of Antiretroviral Therapy (SMART) study in 2006 due to safety concerns around the 250% increase in risk of progression generated by interrupted therapy, clinical guidelines have discouraged treatment interruption and favored the implementation of continuous antiretroviral therapy (The Strategies for Management 2006). Adherence to treatment is also crucial to reducing the rise of drug resistance, as treatment interruption allows HIV to more consistently multiply, thereby increasing the risk of viral mutation and hence production of new, drug-resistant strains. Despite the evidence now in favor of continuous ART from both therapeutic and public health perspectives, ART adherence is not a given for many HIV-infected patients. Reasons for short-term (days to months) interruption or failure of ART vary widely and may include drug toxicity or interaction, poor drug absorption, intolerable side effects, pill burden, financial constraints, lack of access to medication, and a range of other co-morbidities, including psychiatric or medical illnesses (Guy 2013). Thus, due to the potentially insurmountable impact of small alterations to the implementation time t_ϵ, and the degree to which an increased infected macrophage population, serving as a viral reservoir, can drive the system more rapidly to AIDS, we explore how interruption in treatment will influence the time to progression.

To simulate treatment interruptions, we again use the model (2) but redefine $\mathcal{A}(t)$ by

$$\mathcal{A}(t) = 1 - \epsilon \left[H(t - t_\epsilon) - H(t - t_I) + H\left(t - t_R\right) \right],$$

where $H(t)$ is again the Heaviside function, t_ϵ is the time at which ART is first implemented with assumed efficacy ϵ, t_I is the time at which treatment interruption occurs, and t_R is the time at which ART is reinstated. The times t_I and t_R can be further decomposed into

$$t_I = t_\epsilon + D_\epsilon,$$

$$t_R = t_I + D_I,$$

where D_ϵ represents the duration of initial treatment, i.e., the length of time after t_ϵ until treatment is interrupted, and D_I is the duration of the treatment interruption, i.e., the amount of time that a patient remains off of ART until the time of treatment reinstatement, t_R. For instance, if $D_\epsilon = 6$ months, then ART is ceased 6 months after

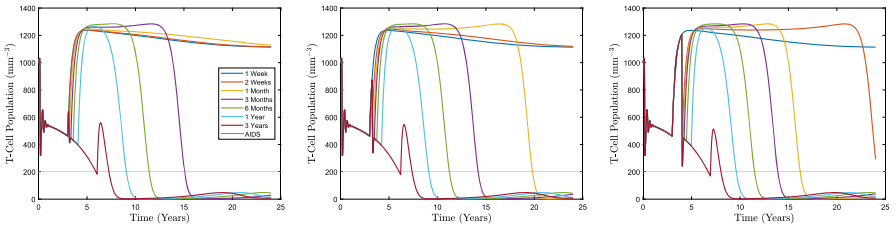

(a) $D_\epsilon = 1$ month **(b)** $D_\epsilon = 3$ months **(c)** $D_\epsilon = 1$ year

Fig. 14 Comparison of T-cell populations subjected to ART interruption with fixed duration of treatment D_ϵ and varied lengths of interruption D_I, the latter represented in the legend as seen in figure (*a*) ($t_\epsilon = 3$ years and $\epsilon = 0.7$)

t_ϵ, while if $D_I = 3$ months, then ART is reinstated 3 months after interruption t_I. In particular, we note that $\mathcal{A}(t)$ only takes on two distinct values and may be written as

$$\mathcal{A}(t) = \begin{cases} 1, & 0 \le t < t_\epsilon \text{ or } t_I \le t < t_R \\ 1-\epsilon, & t_\epsilon \le t < t_I \text{ or } t \ge t_R. \end{cases}$$

In order to study the implications of altering D_ϵ and D_I, we fix the values of the treatment efficacy and time of initiation to $\epsilon = 0.7$ and $t_\epsilon = 3$ years, respectively, throughout all simulations. We note that for other values that were used in previous sections, for instance $t_\epsilon = 3.5$ and $\epsilon = 0.8$, nearly all patients progressed to AIDS within 25 years when treatment was appreciably interrupted. Hence, the aforementioned values were chosen to highlight the outcome differences that may appear due only to treatment interruption. Additionally, though interruptions may lead to the emergence of drug-resistant viral strains, we will neglect such mutations in the current study in order to capture the basic features of the viral rebound phase and its long term effects on patient outcomes.

With this, we first focus on the influence of the duration of interruption by fixing the duration of treatment D_ϵ (thus fixing the time at which ART is interrupted t_I) while varying the values of D_I. The results of these simulations are displayed by Fig. 14 for $D_\epsilon = 1, 3$, and 12 months with differing time courses for values of D_I ranging from 1 week to 3 years. Here, we have primarily concentrated on times during which the T-cell population is rebounding directly after ART is introduced so that D_ϵ is between 2 weeks and 1 year. If ART is interrupted after the T-cell count has been restored to healthy levels of approximately 1000 copies/mm^3, treatment interruption does not drive the system to AIDS unless an individual is off of ART for more than 1 year. Additionally, if ART is interrupted within the first month of initial implementation, the interruption merely acts as an extension of the implementation time t_ϵ. That is, if $D_\epsilon < 1$ month and $D_I < 1$ month, then the effects of treatment interruption are negligible, while if $D_\epsilon < 1$ month, an interruption length D_I between 1 month and 1 year yields the same qualitative outcome as redefining the ART implementation time to $t_\epsilon + D_I$. Therefore, this scenario produces the same behavior as prolonging the implementation time by D_I.

For these reasons, we focus on the effects of interruption during the $D_\epsilon = 1$ month through $D_\epsilon = 1$ year post-ART initiation time frame. Figure 14 shows that for such values of D_ϵ, the time to AIDS remains largely unchanged for a sufficiently large interruption duration ($D_I \geq 3$ months) regardless of treatment duration. However, under an interruption of $D_I = 1$ month, a notable effect arises wherein an initial treatment period of $D_\epsilon = 1$ month does not lead to progression within 25 years, but a longer treatment period of $D_\epsilon = 2$ months or more will cause progression to AIDS, and treatment lasting between $D_\epsilon = 3$ and $D_\epsilon = 12$ months induces an even more rapid progression. Simulations further demonstrated that for a treatment duration of $D_\epsilon = 18$ months or more, a one-month treatment interruption does not progress to AIDS within 25 years. Hence, there is a specific time period of $D_\epsilon = 2$ to $D_\epsilon = 12$ months post-initiation during which patients are particularly sensitive to interruptions in treatment. This effect is likely due to the fact that during the initial stages of ART (within 1-year post-implementation) T-cell populations return to previous healthy levels and thus provide additional target cells for virions. With an increased viral population stemming from treatment interruption and bolstered by reservoirs in the form of infected macrophages, the restoration of the T-cell population provides an hospitable environment for infection and production of new virions. However, if treatment has been continued for a sufficiently long time period (> 1 year), wherein viral reservoirs are appreciably reduced by ART, the increased T-cell population does not give rise to a rapid increase in the number of new infections, due to the depletion of the viral load. This dual dependence on virions and susceptible T-cells creates a non-monotonic influence of D_ϵ on viral explosion.

Such nonlinear responses become evident upon fixing the duration of interruption, D_I at 1 month. Then, as D_ϵ increases over the time course of 1 to 12 months the time to progression decreases. Said another way, interrupting ART during the beginning stages of treatment is not as detrimental as interruption after 1 year on ART. This is displayed by Fig. 14; in particular, by following the yellow curve which represents $D_I = 1$ month. This fixed interruption duration in Fig. 14(a) does not progress to AIDS if ART is interrupted after 1 month of treatment. However, in Figs. 14(b) and 14(c), respectively, if interruption occurs 3 months post-initiation, a progression to AIDS transpires within 20 years, while if interruption occurs after 12 months, an infected patient progresses within 16.5 years.

In order to further illustrate this interruption phenomenon we fix the duration of interruption, $D_I = 1$ month and study the time courses of all relevant populations in the model, seen in Fig. 15. This figure - in particular, Fig. 15(a) - illustrates the decreasing, nonlinear response on the time to progression generated by increasing D_ϵ between 1 and 12 months. After approximately 12 months this effect disappears and the time to AIDS increases instead. This cannot be attributed directly to prior values of the T-cell count, as progression is most rapid when ART is interrupted after 1 year, but this curve does not correspond to the greatest value of $T(t_I)$ or the smallest value of $T(t_R)$. Thus, the nonlinear behavior stems from information contained within a different population.

Therefore, we further study the possible links between one of the populations and this nonlinear behavior, by plotting virion, macrophage, and infected macrophage time courses in Figs. 15(b), 15(c), and 15(d), respectively. Both the virion and macrophage

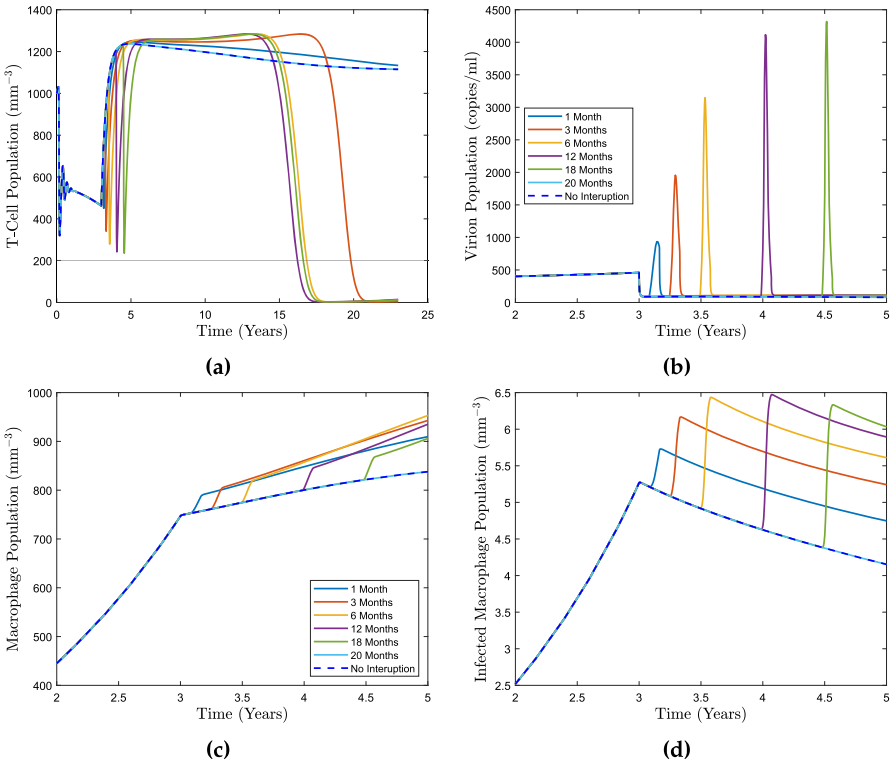

Fig. 15 Comparison of T-cell, virion, macrophage, and infected macrophage populations subject to ART interruption. Here, D_ϵ is varied, while $D_I = 1$ month, $\epsilon = 0.7$, and $t_\epsilon = 3$ years are all fixed. Legends within panels (b) and (c) are valid for all figures

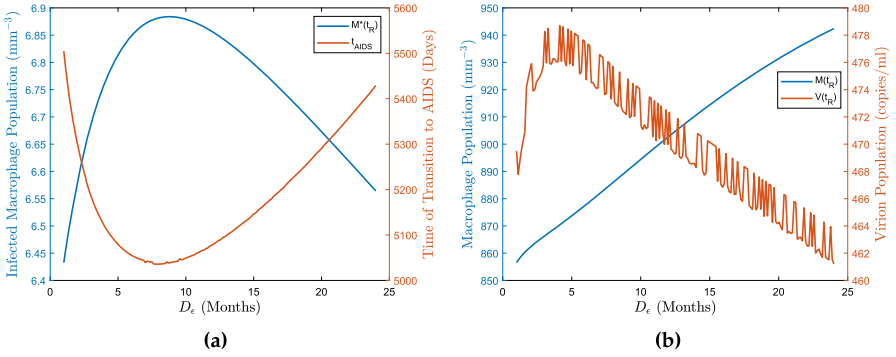

Fig. 16 Comparison of different populations at the time of reimplimentation t_R. Figure (a) represents infected macrophages at t_R compared to the time of progression. Figure (b) represents macrophages and virions at t_R with $D_I = 3$ months, $\epsilon = 0.7$, $t_\epsilon = 3$ years

populations maintain a linearly increasing progression as D_ϵ increases, in particular at the times of interruption t_I and reinstitution t_R. However, Fig. 15(d) demonstrates that the infected macrophage population increases at different rates depending upon D_ϵ. In particular, we expect that the relative density of macrophages and virions at the time of interruption leads to this non-monotonic response in the number of infected macrophages, which are generally responsible for the transition to the final stage of infection. To further verify that infected macrophages are correlated to the pattern caused by interruption of ART, population values at time t_R were plotted as a function of D_ϵ. More specifically, the values $M^*(t_R)$, $M(t_R)$ and $V(t_R)$ were compared to the time at which the disease progresses to AIDS as a function of D_ϵ, seen in Fig. 16. Panel (a) of the figure clearly demonstrates the inversely proportionate relationship between the infected macrophage population at the time of reimplementation, $M^*(t_R)$ and the time of progression to AIDS; namely as the values of $M^*(t_R)$ increase, the time to the development of AIDS necessarily decreases in a nearly identical fashion. As seen in Fig. 16(b) the macrophage and virion populations do not follow the same nonlinear trend as the infected macrophage population and hence, are not directly correlated to this non-monotonic response. We note, in particular, that the oscillatory behavior of the virion population as a function of D_ϵ occurs because of small corresponding oscillations in the infected T-cell population as D_ϵ is altered. Additionally, the T-cell population is not responsible for changes in the time to the onset of AIDS as the viral explosion that leads to this transition are induced by the virions produced from infected macrophages. This is reiterated in Fig. 17 wherein a viral decomposition, in terms of the production mechanism of new virions, is displayed under ART interruption. The figure shows that changes in the number of virions produced by infected macrophages at the time of ART reinstitution drastically impacts the appearance of viral explosion even though the viral load at the time of interruption is identical and the reimplementation of ART initially decreases the viral load to similar levels. Therefore, viral explosion is clearly driven by production of virions from infected macrophages and subtle changes in the values of the infected macrophage population at the time of treatment reinstatement $M^*(t_R)$ are correlated to these nonlinear viral explosion patterns.

Though this behavior was initially identified by fixing values of D_ϵ and varying D_I, similar trends emerge under a variety of D_ϵ and D_I combinations. Hence, we next focus on fixing the duration of interruption, D_I, and varying the time at which ART is interrupted so that D_ϵ is altered. In these simulations, displayed within Fig. 18, the change in interruption duration has a significant effect on the system. In particular, while small breaks of $D_I < 1$ week have no appreciable influence (Fig. 18(a)), extending the duration of interruption by an additional 2 weeks induces a progression to AIDS within 20 years (Fig. 18(b)), and this increase in the time to progression is amplified by further boosting the value of D_I. If the duration of interruption is extended to $D_I = 3$ months as shown in Fig. 18(c), progression to AIDS occurs within 20 years even for infected individuals who had only been initially treated for short time periods, e.g. $D_\epsilon \approx 1$ month. Indeed, only those individuals who have experienced continuously uninterrupted treatment for 3 years or more remain above the clinical threshold for AIDS throughout the 25 year period. Moreover, the progression time again displays a non-monotonic dependence on D_ϵ, as patients who have been on ART for 1 year

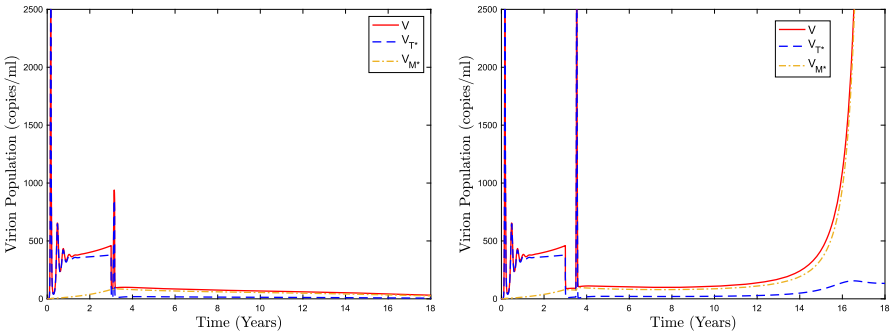

(a) $D_\epsilon = 1$ month **(b)** $D_\epsilon = 6$ months

Fig. 17 Viral decomposition of model undergoing ART interruption with $\epsilon = 0.7$, $t_\epsilon = 3$ years, and $D_I = 1$ month

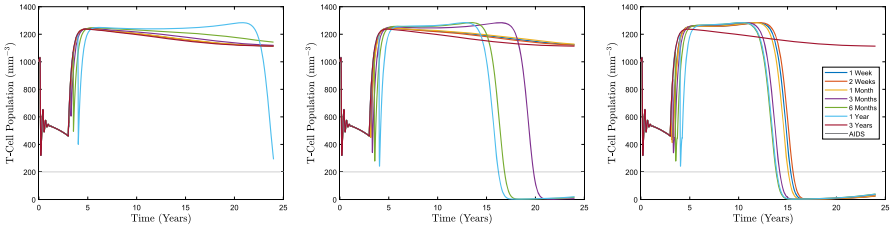

(a) $D_I = 2$ weeks **(b)** $D_I = 1$ month **(c)** $D_I = 3$ months

Fig. 18 Comparison of T-cell populations subjected to ART interruption with fixed duration of interruption D_I and varied lengths of treatment D_ϵ, the latter represented in the legend as seen in panel (c) ($t_\epsilon = 3$ years and $\epsilon = 0.7$)

progress to AIDS faster than those who have been on ART for 6 months, while those who have been on ART for 3 years do not progress to AIDS at all within the 25 year period. Additionally, this effect remains in place for those who experience a treatment interruption lasting $D_I = 1$ month or $D_I = 3$ months.

Thus, we draw two major conclusions. First, the duration of interruption D_I has a more pronounced effect on the time to progression and patient outcomes than does the initial treatment period D_ϵ. More specifically, any interruption period longer than $D_I = 2$ weeks has the ability to induce a progression to AIDS within 25 years. Second, interruption of ART between $D_\epsilon = 6$ months and $D_\epsilon = 12$ months post-implementation significantly increases the probability of progression within the normal human lifespan. This represents a "sweet-spot" for viral proliferation, as ART has suitably restored the strength of the primary infection target (T-cells) and an interruption in treatment triggers a suitably large viral rebound so as to spur additional infection of macrophages prior to the reinstatement of ART. Additionally, the time of progression to AIDS possesses a nonlinear structure that is strongly correlated to the strength of the infected macrophage population at the time of treatment reinstitution, $M(t_R)$.

7 Conclusions and future work

In this paper, a mathematical model for HIV infection, originally proposed within Hernandez-Vargas and Middleton (2013), was formulated to suitably capture all three stages of the disease process while being shown to guarantee both the positivity and boundedness of populations and ensure their limited sensitivity to parameter variations. Additionally, a dynamical analysis of the unique, infection-free steady state was performed, thereby identifying the basic reproduction numbers corresponding to T-cell and macrophage infection. The subtle, but crucial, interplay between these two infection mechanisms was elucidated. This provides further evidence to bolster the idea (Hernandez-Vargas and Middleton 2013) that long-term HIV infection, and in particular, the progression to AIDS via viral explosion, is a multiscale process with differing infection pathways operating at disparate timescales. Here, the infection of T-cells provides the fast dynamics of the system, while the slower, but continued, macrophage infection process ultimately leads to viral explosion and drives the T-cell count below the threshold for AIDS over the course of many years, in many cases, even with the initiation of antiretroviral therapy. A global sensitivity analysis was performed via active subspace methods that demonstrates the importance of immunological recruitment of macrophages (though other classes of viral reservoir can be used) on the progression to AIDS. In particular, this parameter ρ_M does not influence the stability properties of the disease-free state through basic reproduction numbers, but greatly impacts the quantitative behavior of the disease process by partially governing the rate at which an HIV-infected individual undergoes the transition to AIDS. Finally, time-dependent indicator functions were used to study both the introduction of ART on an infected individual and the influence of treatment interruption. While both the drug efficacy and time of initiation influence the time until the onset of AIDS, the latter was demonstrated to be significantly more impactful than the former, further solidifying the significance of consistent testing and early identification of HIV infection. Thus, we reiterate the crucial importance of beginning ART immediately upon receiving a positive diagnosis, as earlier ART implementation yields considerably more desirable outcomes for HIV-infected individuals. Additionally, assuming the presence of an interruption to ART, the time of treatment interruption (via the duration of treatment D_ϵ) was shown to be more impactful to the eventual onset time of AIDS than the duration of interruption D_I. More specifically, variations in the duration of ART prior to interruption induce a nonlinear response in the time to the development of AIDS, as for a three month interruption in ART, treatment durations of one month or twelve months both yield longer AIDS progression times than that of a six month treatment duration. Hence, individuals undergoing antiretroviral therapy are more detrimentally affected by interruptions occurring within the first year of treatment than afterward. This conclusion further reinforces a similar finding in Haering et al. (2014), in which it was determined that ART switching strategies are not beneficial to prolonging the onset of AIDS if initiated more than two years post-infection. In this way, quantitative estimates were provided herein regarding the ability of ART to extend the chronic phase of the disease beyond the expected lifetime of the patient, even in the presence of treatment interruptions.

Though our study has provided a number of new insights, it is by no means exhaustive. In the future, it would be advantageous to expand the scope of the model by incorporating additional complexities; for instance, introducing the effect of viral mutations and more detailed immune responses, thereby providing a more nuanced understanding of the dynamics of HIV infection and treatment. Hence, future work may focus on the impact of different treatment switching strategies, similar to those of Haering et al. (2014) or Hernandez-Vargas et al. (2014), to combat new, and possibly drug-resistant, strains of HIV arising from viral mutation while also incorporating a variety of drug efficacies to study the impact of treatment interruption. As demonstrated herein, interruptions of antiretroviral therapy, even of mild duration, can induce drastic differences in long-term patient outcomes, and the additional emergence of drug-resistant viral mutations would be a particularly critical avenue to explore in the future. Furthermore, an investigation into different interruption patterns and their potential consequences for the efficacy of antiretroviral therapy could provide greater insight into the interplay between the suppression of the viral reservoir and the time to the onset of AIDS. In summary, the introduction of more complex and realistic mathematical models of HIV infection dynamics will improve our general knowledge of patient outcomes affecting treatment scheduling and implementation.

Appendix A: Proofs of Theorems

We first prove the positivity result.

Proof of Theorem 1 Assume $T(0), M(0), V(0) > 0$ and $T^*(0), M^*(0) \geq 0$. Define

$$\tau_\infty = \sup\{s > 0 : T(s), M(s), V(s) > 0\}.$$

Due to the continuity of these functions, we find $\tau_\infty > 0$. Then, for $t \in [0, \tau_\infty)$ we have

$$\dot{T}^*(t) \geq -\delta_{T^*} T^*(t)$$

from (1) and upon multiplying by $e^{\delta_{T^*} t}$ and integrating, we find

$$\frac{d}{dt}\left(T^*(t) e^{\delta_{T^*} t}\right) \geq 0,$$

and thus

$$T^*(t) \geq T^*(0) e^{-\delta_{T^*} t} \geq 0$$

on this interval. Analogously, the same analysis yields

$$M^*(t) \geq M^*(0) e^{-\delta_{M^*} t} \geq 0$$

for $t \in [0, \tau_\infty)$. This idea can also be applied to $V(t)$ to find

$$V(t) \geq V(0)e^{-\delta_V t} > 0$$

for $t \in [0, \tau_\infty)$.

To obtain lower bounds on the remaining compartments, we will first need to establish upper bounds on these quantities. In particular, letting

$$S(t) = T(t) + T^*(t),$$

and adding the equations for T and T^* gives

$$\begin{aligned}\dot{S}(t) &= s_T + \frac{\rho_T V}{c_T + V} T(t) - \delta_T T(t) - \delta_{T^*} T^*(t) \\ &\leq s_T + \rho_T T(t) - \delta_T T(t) - \delta_{T^*} T^*(t) \\ &\leq s_T + \rho_T S(t)\end{aligned}$$

for $t \in [0, \tau_\infty)$. With this, we have a linear differential inequality and, upon multiplying by $e^{-\rho_T t}$ and integrating, we find

$$S(t) \leq \left(S(0) + \frac{s_T}{\rho_T} \right) e^{\rho_T t}.$$

As both $T(t)$ and $T^*(t)$ are positive on $[0, \tau_\infty)$, the upper bound on $S(t)$ further implies

$$T(t) \leq \left(S(0) + \frac{s_T}{\rho_T} \right) e^{\rho_T t}$$

and

$$T^*(t) \leq \left(S(0) + \frac{s_T}{\rho_T} \right) e^{\rho_T t}$$

for $t \in [0, \tau_\infty)$. An analogous argument can be applied to $M(t)$ and $M^*(t)$ to find

$$M(t) \leq \left(P(0) + \frac{s_M}{\rho_M} \right) e^{\rho_M t}$$

and

$$M^*(t) \leq \left(P(0) + \frac{s_M}{\rho_M} \right) e^{\rho_M t}$$

where

$$P(t) = M(t) + M^*(t).$$

These upper bounds imply the same for the viral compartment, namely

$$\dot{V}(t) \leq p_T \left(S(0) + \frac{s_T}{\rho_T} \right) e^{\rho_T t} + p_M \left(P(0) + \frac{s_M}{\rho_M} \right) e^{\rho_M t},$$

and upon integrating, we arrive at an exponential upper bound

$$V(t) \leq C_0 e^{\alpha t}$$

where

$$C_0 = \max \left\{ V(0), \frac{p_T}{\rho_T} \left(S(0) + \frac{s_T}{\rho_T} \right) + \frac{p_M}{\rho_M} \left(P(0) + \frac{s_M}{\rho_M} \right) \right\}$$

and $\alpha = \max\{\rho_T, \rho_M\}$.

Finally, with the upper bound on $V(t)$, we can lower bound the $T(t)$ and $M(t)$ compartments. More specifically, using the upper bound on $V(t)$ in the equation for $T(t)$ yields

$$\dot{T}(t) \geq -k_T C_0 e^{\alpha t} T(t) - \delta_T T(t) \geq -C_1 \left(1 + e^{\alpha t}\right) T(t)$$

for $t \in [0, \tau_\infty)$ where $C_1 = \max\{k_T C_0, \delta_T\}$. Using an integrating factor as before, then yields

$$\frac{d}{dt} \left[T(t) \exp \left(C_1 \int_0^t (1 + e^{\alpha s})\, ds \right) \right] \geq 0$$

and

$$T(t) \geq T(0) \exp \left(-C_1 \int_0^t (1 + e^{\alpha s})\, ds \right) > 0$$

for $t \in [0, \tau_\infty)$. The same argument applies directly to $M(t)$ so that

$$M(t) \geq M(0) \exp \left(-C_2 \int_0^t (1 + e^{\alpha s})\, ds \right) > 0$$

for $t \in [0, \tau_\infty)$, where $C_2 = \max\{k_M C_0, \delta_M\}$. Finally, if $\tau_\infty < \infty$ then the exponentially decreasing lower bounds on $T(t)$, $M(t)$, and $V(t)$ imply that each is strictly positive at τ_∞. This contradicts the maximality of τ_∞. Hence, $\tau_\infty = \infty$ and each function must remain positive for all $t \geq 0$. Furthermore, the nonnegativity of $T^*(t)$ and $M^*(t)$ are maintained for $t \in [0, \infty)$ as shown above. □

We may use similar tools to derive the steady states of the model.

Proof of Theorem 2 In order to determine time-independent solutions, the time derivatives in (1) are set to zero, and we solve for each population. Doing so yields

$$\begin{cases} 0 = s_T + \dfrac{\rho_T V}{c_T + V} T - k_T T V - \delta_T T \\ T^* = \dfrac{k_T}{\delta_{T^*}} T V \\ 0 = s_M + \dfrac{\rho_M V}{c_M + V} M - k_M M V - \delta_M M \\ M^* = \dfrac{k_M}{\delta_{M^*}} M V \\ V = \dfrac{p_T}{\delta_V} T^* + \dfrac{p_M}{\delta_V} M^*. \end{cases} \tag{3}$$

From the second and fourth equations, taking $V = 0$ directly implies $T^* = M^* = 0$. Upon simplifying the first and third equations using $V = 0$, the unique uninfected steady state is obtained.

Turning to the uninfected steady state, we insert the second and fourth equations into the final equation in (3). Assuming $V \neq 0$, the result is

$$\frac{p_T k_T}{\delta_V \delta_{T^*}} T + \frac{p_M k_M}{\delta_V \delta_{M^*}} M = 1.$$

This equation is then solved for M to obtain a linear dependence on T and inserted into the third equation of (3) to provide a quadratic equation in the T and V variables. As $c_T + V > 0$, we can multiply by this term throughout the first equation above and solve for the steady-state T-cell count in terms of V, namely

$$T = \frac{s_T (c_T + V)}{\delta_T c_T - (\rho_T - k_T c_T - \delta_T) V + k_T V^2}.$$

This is then inserted into the quadratic equation in T and V to obtain a quartic equation in V only, which can be reduced to the form

$$\alpha_4 V^4 + \alpha_3 V^3 + \alpha_2 V^2 + \alpha_1 V + \alpha_0 = 0 \tag{4}$$

where

$$\begin{aligned} \alpha_4 &= -\frac{k_T \delta_V \delta_{M^*}}{p_M}, \\ \alpha_3 &= \frac{s_T k_T p_T \delta_{M^*}}{p_M \delta_{T^*}} + \frac{\delta_V \delta_{M^*}}{p_M} (\rho_T - k_T c_T - \delta_T) \\ &\quad + k_T \left[s_M + (\rho_M - k_M c_M - \delta_M) \frac{\delta_V \delta_{M^*}}{k_M p_M} \right], \\ \alpha_2 &= \frac{s_T c_T k_T p_T \delta_{M^*}}{p_M \delta_{T^*}} - s_T (\rho_M - k_M c_M - \delta_M) + k_T \left(s_M c_M - \frac{c_M \delta_M \delta_{M^*} \delta_V}{k_M p_M} \right) \end{aligned}$$

$$
\begin{aligned}
&-\frac{c_T\delta_T\delta_{M^*}\delta_V}{p_M}-\left[s_M+(\rho_M-k_Mc_M-\delta_M)\,\frac{\delta_{M^*}\delta_V}{k_Mp_M}\right](\rho_T-k_Tc_T-\delta_T)\,,\\
\alpha_1 &= c_T\delta_T\left[s_M+(\rho_M-k_Mc_M-\delta_M)\,\frac{\delta_V\delta_{M^*}}{k_Mp_M}\right]\\
&\quad -c_M\left(s_M-\frac{\delta_M\delta_{M^*}\delta_V}{k_Mp_M}\right)(\rho_T-k_Tc_T-\delta_T)\\
&\quad -s_Tc_T\,(\rho_M-k_Mc_M-\delta_M)+\frac{s_Tk_Tp_Tc_M\delta_M\delta_{M^*}}{k_Mp_M\delta_{T^*}},\\
\alpha_0 &= c_Tc_M\left(\delta_T\left[s_M-\frac{\delta_M\delta_{M^*}\delta_V}{k_Mp_M}\right]+\frac{s_Tk_Tp_T\delta_M\delta_{M^*}}{k_Mp_M\delta_{T^*}}\right).
\end{aligned}
$$

Descartes' Rule of Signs can be used to determine conditions on α_0, α_1, α_2, and α_3 that guarantee one sign change amongst consecutive coefficients, and thus exactly one positive, real solution. However, in simulating steady state solutions over a 10% (or greater) parameter variation, we have determined that two, or even four, positive solutions often arise, and these may be generally associated with the two distinct infected steady states in the reduced model of Pankavich et al. (2020). □

Finally, we prove the stability result.

Proof of Theorem 3 Recalling the unique uninfected steady state

$$E_{NI}=\left(\frac{s_T}{\delta_T},0,\frac{s_M}{\delta_M},0,0\right),$$

we compute the eigenvalues of the Jacobian matrix of (1) to determine the stability properties of the equilibrium. In particular, we will identify conditions which ensure that all eigenvalues have negative real part, and thus imply E_{NI} is stable. Denoting population values by $y_1,\ldots,y_5$ and computing the Jacobian of the right side of (1) yields

$$
J=\begin{bmatrix}
\frac{\rho_Ty_5}{c_T+y_5}-k_Ty_5-\delta_T & 0 & 0 & 0 & \left(\frac{-\rho_Ty_5}{(c_T+y_5)^2}+\frac{\rho_T}{c_T+y_5}\right)y_1-k_Ty_1\\
k_Ty_5 & -\delta_{T^*} & 0 & 0 & k_Ty1\\
0 & 0 & \frac{\rho_My_5}{c_M+y_5}-k_My_5-\delta_M & 0 & \left(\frac{-\rho_My_5}{(c_M+y_5)^2}+\frac{\rho_M}{c_M+y_5}\right)y_3-k_My_3\\
0 & 0 & k_My_5 & -\delta_{M^*} & k_My_3\\
0 & p_T & 0 & p_M & -\delta_V
\end{bmatrix} \tag{5}
$$

The Jacobian is then evaluated at E_{NI}, resulting in the constant 5×5 matrix

$$
J(E_{NI})=\begin{bmatrix}
-\delta_T & 0 & 0 & 0 & \left(\frac{\rho_T}{c_T}-k_T\right)\frac{s_T}{\delta_T}\\
0 & -\delta_{T^*} & 0 & 0 & k_T\frac{s_T}{\delta_T}\\
0 & 0 & -\delta_M & 0 & \left(\frac{\rho_M}{c_M}-k_M\right)\frac{s_M}{\delta_M}\\
0 & 0 & 0 & -\delta_{M^*} & k_M\frac{s_M}{\delta_M}\\
0 & p_T & 0 & p_M & -\delta_V
\end{bmatrix} \tag{6}
$$

and upon computing the characteristic polynomial, we find

$$\begin{aligned}|J(E_{NI}) - \lambda\mathbb{I}| = &-(\delta_T + \lambda)(\delta_{T^*} + \lambda)(\delta_M + \lambda)(\delta_{M^*} + \lambda)(\delta_V + \lambda) \\ &+ (\delta_T + \lambda)(\delta_{T^*} + \lambda)(\delta_V + \lambda)\frac{p_M k_M s_M}{\delta_M} \\ &+ (\delta_T + \lambda)(\delta_M + \lambda)(\delta_{M^*} + \lambda)\frac{p_T k_T s_T}{\delta_T}.\end{aligned}$$

The common factors $(\delta_T + \lambda)$ and $(\delta_M + \lambda)$ can be removed from each term and correspond to the negative, real eigenvalues

$$\lambda = -\delta_T \qquad \text{and} \qquad \lambda = -\delta_M.$$

Solving for the roots of the remaining polynomial leads directly to

$$0 = -(\delta_{T^*} + \lambda)(\delta_{m^*} + \lambda)(\delta_v + \lambda) + (\delta_{T^*} + \lambda)R_M\delta_{M^*}\delta_V + (\delta_{m^*} + \lambda)R_T\delta_{T^*}\delta_V$$

where

$$R_M = \frac{p_M k_M s_M}{\delta_M \delta_{M^*}\delta_V} \qquad \text{and} \qquad R_T = \frac{p_T k_T s_T}{\delta_T \delta_{T^*}\delta_V}.$$

Finally, this is a cubic equation of the form

$$\lambda^3 + a_2\lambda^2 + a_1\lambda + a_0 = 0$$

where

$$\begin{aligned}a_2 &= \delta_{T^*} + \delta_{M^*} + \delta_V, \\ a_1 &= \delta_{T^*}\delta_{M^*} + (1 - R_M)\delta_{M^*}\delta_V + (1 - R_T)\delta_{T^*}\delta_V,\end{aligned}$$

and

$$a_0 = \delta_V\delta_{T^*}\delta_{M^*}\left(1 - R_M - R_T\right).$$

Using the Routh-Hurwitz Criteria, the roots of this equation will all possess negative real part when

$$a_2 > 0, \qquad a_0 > 0, \qquad \text{and} \qquad a_2 a_1 > a_0.$$

Due to the positivity of the parameters, the first condition is trivially satisfied. The second condition clearly requires the stated inequality, namely

$$R_T + R_M < 1,$$

which further implies the last condition, as

$$a_2 a_1 > \delta_V \delta_{T^*} \delta_{M^*} > a_0$$

for $0 < R_M + R_T < 1$. Thus, E_{NI} is stable under this condition, and unstable if

$$R_T + R_M > 1,$$

which implies the existence of a root with positive real part under the same argument. □

Appendix B: Active subspaces

In the final appendix, we provide a brief description of the gradient-based active subspace method (Russi 2010) used to analyze $\mathcal{T}(5;\, p)$, $\mathcal{T}(10;\, p)$, and $\mathcal{F}(p)$. In addition to the current discussion, the method has also been recently summarized within Constantine (2015). First, we normalize the values of input parameters. Thus, while p represents the vector of varying parameters, let $q \in Q = [-1, 1]^{15}$ denote the vector of *normalized* input parameters, where Q represents the space of *normalized* parameter values. Namely, we assume that the independent inputs have been shifted and scaled so that they are centered at the origin and possess unit variation. Additionally, assume that a quantity of interest $g(q)$ has been selected, and the input space is equipped with a probability density function $\psi(q)$ that is strictly positive in the domain of $g(q)$, zero outside the domain, and normalized so that $\int_Q \psi(q)\, dq = 1$. In practice, ψ identifies the set of input parameters of interest and quantifies their variability. We choose ψ so that each parameter is uniformly distributed on an interval determined by a 10% variation of its baseline value. For instance, the baseline value of s_T is 10, and thus we consider uniformly-distributed parameter variations satisfying $9 \leq s_T \leq 11$ within the construction of $\psi(q)$. Assume that $g : Q \to \mathbb{R}$ is continuous, square-integrable with respect to the weight ψ, and differentiable with gradient vector $\nabla g \in \mathbb{R}^{15}$, which is also square-integrable with respect to ψ. The active subspace is then defined by the first $n < 15$ eigenvectors of the 15×15 symmetric positive semi-definite matrix

$$C = \int_Q \nabla g(q) \nabla g(q)^T \psi(q)\, dq =: W \Lambda W^T, \tag{7}$$

where the right side of (7) represents the spectral decomposition of C (Axler (1997); Pankavich (2020)). Said another way, W represents the orthogonal matrix whose columns w_ℓ, $(\ell = 1, \ldots, 15)$ are the orthonormal eigenvectors of C, and Λ is the diagonal matrix of eigenvalues of C, denoted $\lambda_1, \ldots, \lambda_{15}$. The matrix C represents an average derivative functional which weights input values according to the probability density ψ. Within this decomposition, the eigenvalues in Λ, which must be non-negative, are listed in descending order and the associated eigenvectors are listed within the same column as their corresponding eigenvalues.

The eigenvalue λ_ℓ measures the average change in g subject to perturbations in q along the direction corresponding to the eigenvector w_ℓ, as these quantities are related by the identity

$$\lambda_\ell = \int_Q |\nabla g(q) \cdot w_\ell|^2 \psi(q)\, dq \tag{8}$$

for $\ell = 1, \ldots, 15$. For example, if $\lambda_\ell = 0$, then g is constant along the direction w_ℓ, and directions along which g is constant can be essentially ignored when studying the behavior of g under changes in the parameter space Q. Conversely, if the eigenvalue under consideration is large, then we may deduce from (8) that g changes considerably in the direction of the corresponding eigenvector. Now, suppose that a spectral gap exists and the first $n < 15$ eigenvalues are significantly larger than the trailing $15 - n$. Let W_1 be the matrix containing the first n columns of W. Then, as we will show below, a reasonable approximation for g is $g(q) \approx h(W_1^T q)$, where h is the projection of g onto the range of W_1, i.e. $h(y) = g(W_1 y)$.

Once the eigendecomposition involving W and Λ in (7) has been determined, the eigenvalues and eigenvectors can be separated as

$$\Lambda = \begin{bmatrix} \Lambda_1 & 0 \\ 0 & \Lambda_2 \end{bmatrix}, \quad W = \begin{bmatrix} W_1 & W_2 \end{bmatrix} \tag{9}$$

where Λ_1 contains the larger eigenvalues of C, Λ_2 contains the smaller eigenvalues, and W_k contains the eigenvectors associated with each Λ_k, for $k = 1, 2$. A simple way to differentiate between the larger and smaller eigenvalues is to list them on a log plot from greatest to least and determine the appearance of a spectral gap. This gap will correspond to differences of at least an order of magnitude, allowing us to compartmentalize the greatest eigenvalues within Λ_1 and the remaining, lesser eigenvalues in Λ_2. A more systematic method of choosing the number of eigenvalues to store within Λ_1 can also be utilized, as developed in Constantine (2015).

With the decomposition (9), we can represent any normalized parameter q by

$$q = \underbrace{W W^T}_{=I} q = W_1 \underbrace{W_1^T q}_{=r} + W_2 \underbrace{W_2^T q}_{=s} = W_1 r + W_2 s. \tag{10}$$

Hence, evaluating the quantity of interest at the point q is equivalent to doing so at $W_1 r + W_2 s$, and we can approximate $g(q)$ using

$$g(q) = g(W_1 r + W_2 s) \approx g(W_1 r) = g(W_1 W_1^T q) = h(W_1^T q).$$

By the definition of W_1 and W_2, we see that small perturbations in s will not, on average, alter the values of g. However, small perturbations in r will, on average, change g significantly. Hence, the outputs of W_1 are defined to be the *active subspace* of the model and the outputs of W_2 are the corresponding *inactive subspace*. The linear combinations that generate these subspaces then represent the contributions of

differing parameters in the model and describe the sensitivity of the quantity of interest with respect to parameter variations.

In general, the eigenvalues and eigenvectors of C defined by (7) can be well-approximated computationally, using finite difference methods and Monte Carlo sampling. Though we only briefly outline the method below, full details can be found in Constantine (2015) (Algorithm 3.1) and Constantine and Gleich (2014). The numerical algorithm can be described concisely as follows:

1. Draw N parameter samples $\{q_j\}_{j=1}^N$ independently according to the density ψ.
2. For each parameter sample q_j, compute the gradient $\nabla_q g_j = \nabla_q g(p_j)$ for each entry $i = 1, .., 15$ by using the finite difference approximation

$$\partial_{q_i} g(q_j) \approx \frac{g(q_j + \epsilon_i) - g(q_j)}{|\epsilon_i|}$$

   where $(\epsilon_i)_k = \Delta \delta_{ik}$ represents a vector perturbation from the sampled parameter values, δ_{ik} is the Kronecker delta, and $\Delta > 0$ can be taken as small as desired.
3. Approximate the matrix C by the finite sum

$$C \approx \hat{C} = \frac{1}{N} \sum_{j=1}^{N} (\nabla_q g_j)(\nabla_q g_j)^T$$

4. Compute the corresponding eigendecomposition $\hat{C} = \hat{W} \hat{\Lambda} \hat{W}^T$.

In practice, we take $N \approx 1000$ sets of parameter samples from Q. Once $\hat{W}$ and $\hat{\Lambda}$ are computed, the eigenspace is decomposed into its active and inactive portions, namely $\hat{W}_1$ and $\hat{W}_2$, which correspond to the set of eigenvectors associated with the large eigenvalues along the diagonal of $\hat{\Lambda}_1$ and the small eigenvalues along the diagonal of $\hat{\Lambda}_2$, respectively. In practice, many systems possess a one-dimensional active subspace, so that $\hat{\Lambda}_1 \in \mathbb{R}$ and $\hat{W}_1 = w \in \mathbb{R}^m$. In such a scenario, the values of the vector w represent the weights in a linear combination of the input parameters along which the quantity of interest is most variable. In this way, the entries of w describe the relative importance of the parameters with respect to this quantity. For instance, if $w_2 \gg w_1$, then we generally expect $g(q)$ to vary more when the second entry of q is altered from the w direction than when the first entry of q is altered. Similarly, if say $w_3 \approx 0$ then $g(q)$ does not change much on average when the third entry of q is altered. With this information, the ultimate goal is to produce a model possessing reduced dimensional dependence, and this can be done using a *sufficient summary plot*. In particular, if the active subspace is one-dimensional, then we have identified the single direction in the parameter space along which g is most variable, and the Monte Carlo sample points $\{q_j\}_{j=1}^N$ are used to construct an approximate model h along this direction, given by $w^T q$. To create the reduced model, a simple linear fit, or if greater precision is required a nonlinear least-squares curve fit, can be used. This method has previously been utilized to study the global sensitivity of parameters within a variety of scientific models (Constantine and Diaz 2017; Constantine and

Doostan 2017; Diaz et al. 2018; Martinez et al. 2022; Pankavich and Loudon 2017; Shutt et al. 2017; Terrab and Pankavich 2020, 2022).

References

Axler S (1997) Linear algebra done right. Springer, Berlin

Brown A, Zhang H, Lopez P, Pardo C, Garnter S (2006) In vitro modeling of the HIV-macrophage reservoir. J Leukoc Biol 80(5):1127–1135

Callaway DS, Perelson A (2002) HIV-1 infection and low steady state viral loads. Bull Math Biol 64:29–64

Centers for Disease Control and Prevention (CDC.gov), Frequency of HIV Testing and Time from Infection to Diagnosis (Apr 2019). https://www.cdc.gov/nchhstp/newsroom/2017/HIV-testing-and-time-from-infection-to-diagnosis-press-release.html

Constantine P (2015) Active subspaces: emerging ideas for dimension reduction in parameter studies. SIAM, Philadelphia

Constantine P, Diaz P (2017) Global sensitivity metrics from active subspaces. Reliab Eng Syst Saf 162:1–13

Constantine P, Doostan A (2017) Time-dependent global sensitivity analysis with active subspaces for a lithium ion battery model. Stat Anal Data Min ASA Data Sci J 10(5):243–262

Constantine P, Gleich D (2014) Computing active subspaces with Monte Carlo, arXiv:1408.0545

Crepaz N, Song R, Lyss S, Hall H (2021) Estimated time from HIV infection to diagnosis and diagnosis to first viral suppression during 2014–2018. AIDS 35(13):2181–2190

De Boer R, Ribeiro R, Perelson A (2010) Current estimates for HIV-1 production imply rapid viral clearance in lymphoid tissues. PLoS Comput Biol 6(9):e1000906

Diaz P, Constantine P, Kalmbach K, Jones E, Pankavich S (2018) A modified SEIR model for the spread of Ebola in Western Africa and metrics for resource allocation. Appl Math Comput 324:141–155

Gavegnano C, Schinazi R (2009) Antiretroviral therapy in macrophages: implication for HIV eradication. Antivir Chem Chemother 20(2):63–78

Gavegnano C, Fromentin E, Schinazi R (2008) Lower levels of nucleoside analog triphosphates in primary human macrophages compared to human lymphocytes could impair potency of antiretroviral drugs in human viral reservoirs. Global Antiviral J 4:70

R. Guy et al on behalf of Australia HIV Observational Database (AHOD) and Treat Asia HIV Observation Database (TAHOD) (2013) Antiretroviral treatment interruption and loss to follow-up in two HIV cohorts in Australia and Asia: implications for test and treatment prevention strategy. AIDS Patient Care STDs 27(12):681–691. https://doi.org/10.1089/apc.2012.0439

Hadjiandreou M, Conejeros R, Vassiliadis V (2007) Towards a Long-Term Model construction for the dynamic simulation of HIV infection. Math Biosci Eng 4(3):489–504

Haering M, Hördt M, Meyer-Hermann M, Hernandez-Vargas EA (2014) Computational study to determine when to initiate and alternate therapy in HIV infection. BioMed Res Int

Hernandez-Vargas EA, Middleton RH (2013) Modeling the three stages in HIV infection. J Theor Biol 320:33–40

Hernandez-Vargas EA, Colaneri P, Middleton RH (2014) Switching strategies to mitigate HIV mutation. IEEE Trans Control Syst Technol 22(4):1623–1628. https://doi.org/10.1109/TCST.2013.2280920

Hogue I, Bajaria S et al (2008) The dual role of dendritic cells in the immune response to human immunodeficiency virus type 1 infection. J Gen Virol 89:2228–2239

Jones E, Roemer P, Pankavich S, Raghupathi M (2014) Analysis and simulation of the three-component model of HIV dynamics. SIURO 2:308–331

Kirschner D (1996) Using mathematics to understand HIV immune dynamics. Not AMS 43:191–202

Kirschner D, Perelson A (1995) A model for the immune system response to HIV: AZT Treatment Studies, Santa Fe Institute working paper

Koppensteiner H, Brack-Werner R, Schindler M (2012) Macrophages and their relevance in Human Immunodeficiency Virus Type I infection. Retrovirology 9(82):1–11. https://doi.org/10.1186/1742-4690-9-82

Lau J, Smith M, Lewin S, McMahon J (2019) Clinical trials of antiretroviral treatment interruption in HIV-infected individuals. AIDS 33(5):773–791

Lee F, Amin J, Carr A (2014) Efficacy of initial antiretroviral therapy for HIV-1 infection in adults: a systematic review and meta-analysis of 114 studies with up to 144 weeks' follow-up. PLoS ONE 9:e97482

Martinez K, Pankavich S, Brown G (2022) Spatially-heterogeneous embedded stochastic SEIR models for the 2014–2016 Ebola outbreak in West Africa. Spatial Spatio-temporal Epidemiol 41:100505

McGee B, Smith N, Aweeka F (2006) HIV pharmacology: barriers to the eradication of HIV from the CNS. HIV Clin Trials 7:142–153

Minority HIV Fund (HIV.gov), Management of the Treatment-Experienced Patient, (Jan 2022), https://clinicalinfo.hiv.gov/en/guidelines/hiv-clinical-guidelines-adult-and-adolescent-arv/discontinuation-or-interruption

Mitchell B, Laws E, Ndhlovu L (2019) Impact of myeloid reservoirs in HIV cure trials. Curr HIV/AIDS Rep 16(2):129–140

National Institute of Allergy and Infectious Diseases (niaid.nih.gov), 10 Things to Know About HIV Suppression (June 2020). https://www.niaid.nih.gov/diseases-conditions/10-things-know-about-hiv-suppression

Nowak M, May R (2000) Virus dynamics: mathematical principles of immunology and virology. Oxford University Press, Oxford

Orenstein J (2001) The macrophage in HIV infection. Immunobiology 204(5):598–602

Pankavich S (2020) Linear Vector Spaces & Applications, https://hdl.handle.net/11124/174218, 2020-12-01

Pankavich S (2016) The effects of latent infection on the dynamics of HIV. Differ Equ Dyn Syst 24(3):281–303

Pankavich S, Loudon T (2017) Mathematical analysis and dynamic active subspaces for a long term model of HIV. Math Biosci Eng 14(3):709–733

Pankavich S, Parkinson C (2016) Mathematical analysis of an in-host model of viral dynamics with spatial heterogeneity. Discrete Contin Dyn Syst B 21(4):1237–1257

Pankavich S, Neri N, Shutt D (2020) Bistable dynamics and Hopf bifurcation in an early stage model of HIV infection. Discrete Contin Dyn Syst B 25(8):2867–2893

Pankavich S, Shutt D (2015) An in-host model of HIV incorporating Latent Infection and Viral Mutation, Dynamical Systems, Differential Equations, and Applications, AIMS Proceedings, pp 913–922

Perelson A, Nelson P (1999) Mathematical analysis of HIV-1 dynamics in vivo. SIAM Rev 41:3–44

Rong L, Feng Z, Perelson A (2007) Emergence of HIV-1 drug resistance during antiretroviral treatment. Bull Math Biol 69(6):2027–2060

Russi T (2010) Uncertainty quantification with experimental data and complex system models, Ph.D. thesis, UC Berkeley

Shutt D, Manore C, Pankavich S, Porter A, Del Valle S (2017) Estimating the reproductive number, total outbreak size, and reporting rates for Zika epidemics in South and Central America. Epidemics 21:63–79. https://doi.org/10.1016/j.epidem.2017.06.005

Terrab S, Pankavich (2020) sterrab/GSA_PlasmaInstabilities: Initial release, Zenodo, https://doi.org/10.5281/zenodo.4279977

Terrab S, Pankavich S (2022) Global sensitivity analysis of plasma instabilities via active subspaces, arXiv:2106.08552

The Strategies for Management of Antiretroviral Therapy (SMART) Study Group (2006) $CD4^+$ count-guided interruption of antiretroviral treatment. N Engl J Med 355(22):2283–2296. https://doi.org/10.1056/NEJMoa062360

van Sighem A, Nakagawa F, De Angelis D et al (2015) Estimating HIV incidence, time to diagnosis, and the undiagnosed HIV epidemic using routine surveillance data. Epidemiology 26(5):653–660

What to Start (HIV.gov), Initial Combination Antiretroviral Regimens for People with HIV, (Sep 2022), https://clinicalinfo.hiv.gov/en/guidelines/hiv-clinical-guidelines-adult-and-adolescent-arv/what-start-initial-combination-regimens

World Health Organization (2023) (www.who.int), HIV and AIDS (July 2023). https://www.who.int/news-room/fact-sheets/detail/hiv-aids

Xia X (2007) Modelling of HIV infection: vaccine readiness, drug effectiveness and therapeutical failures. J Process Control 17(3):253–260